

UNDERWATER CHANNEL MODELING FOR SONAR APPLICATIONS

A THESIS SUBMITTED TO
THE GRADUATE SCHOOL OF NATURAL AND APPLIED SCIENCES
OF
MIDDLE EAST TECHNICAL UNIVERSITY

BY

ERDAL EPÇAÇAN

IN PARTIAL FULFILLMENT OF THE REQUIREMENTS
FOR
THE DEGREE OF MASTER OF SCIENCE
IN
ELECTRICAL AND ELECTRONICS ENGINEERING

FEBRUARY 2011

Approval of the thesis:

UNDERWATER CHANNEL MODELING FOR SONAR APPLICATIONS

submitted by **ERDAL EPÇAÇAN** in partial fulfillment of the requirements for the degree of **Master of Science in Electrical and Electronics Engineering Department, Middle East Technical University** by,

Prof. Dr. Canan Özgen
Dean, Graduate School of **Natural and Applied Sciences**

Prof. Dr. İsmet Erkmen
Head of Department, **Electrical and Electronics Engineering**

Assoc. Prof. Dr. Tolga Çiloğlu
Supervisor, **Electrical and Electronics Engineering Dept., METU**

Examining Committee Members:

Prof. Dr. Mustafa Kuzuoğlu
Electrical and Electronics Engineering Dept., METU

Assoc. Prof. Dr. Tolga Çiloğlu
Electrical and Electronics Engineering Dept., METU

Assoc. Prof Dr. Çağatay Candan
Electrical and Electronics Engineering Dept., METU

Assoc. Prof Dr. Ali Özgür Yılmaz
Electrical and Electronics Engineering Dept., METU

Tevfik Bahadır Sarıkaya (M.Sc.)
ASELSAN

Date:

I hereby declare that all information in this document has been obtained and presented in accordance with academic rules and ethical conduct. I also declare that, as required by these rules and conduct, I have fully cited and referenced all material and results that are not original to this work.

Name, Last Name: ERDAL EPÇAÇAN

Signature :

ABSTRACT

UNDERWATER CHANNEL MODELING FOR SONAR APPLICATIONS

Epçaçan, Erdal

M.Sc., Department of Electrical and Electronics Engineering

Supervisor : Assoc. Prof. Dr. Tolga Çilođlu

February 2011, 70 pages

Underwater acoustic channel models have been studied in the context of communication and sonar applications. Acoustic propagation channel in an underwater environment exhibits multipath, time-variability and Doppler effects. In this thesis, multipath fading channel models, underwater physical properties and sound propagation characteristics are studied. An underwater channel model for sonar applications is proposed. In the proposed model, the physical characteristics of underwater environment are considered in a comprehensive manner. Experiments/simulations were carried out using real-life data. Model parameters are estimated for a specific location, scenario and physical conditions. The channel response is approximated by fitting the model output to the recorded data. The optimization and estimation are conducted in frequency domain using Mean Square Error criterion.

Keywords: Underwater Acoustic Channel, Fading Channel, Channel Simulation, Parameter Optimization

ÖZ

SONAR UYGULAMALARI İÇİN SUALTI KANAL MODELLEMESİ

Epçaçan, Erdal

Yüksek Lisans, Elektrik ve Elektronik Mühendisliği Bölümü

Tez Yöneticisi : Doç. Dr. Tolga Çiloğlu

Şubat 2011, 70 sayfa

Sualtı akustik kanal modelleri iletişim ve sonar uygulamaları bağlamında incelenmiştir. Sualtı ortamındaki akustik yayılma kanalı çok yollu yayılım, zaman değişkenliği ve Doppler etkisi özelliklerini sergilemektedir. Bu tezde, çok yollu sönümlenen kanal modelleri, sualtı fiziksel özellikleri ve ses yayılım özellikleri incelenmiştir. Sonar uygulamaları için bir sualtı kanal modeli önerilmiştir. Önerilen modelde, sualtı ortamının fiziksel özellikleri kapsamlı bir şekilde göz önünde bulundurulmuştur. Deneyler/simülasyonlar gerçek hayat verileri kullanılarak gerçekleştirilmiştir. Model parametreleri belirli bir konum, senaryo ve fiziksel koşullar için tahmin edilmiştir. Model çıktısı kaydedilmiş verilerle uyuşturularak kanalın dürtü yanıtı yaklaşık olarak bulunmuştur. Optimizasyon ve tahmin işlemleri Ortalama Kare- sel Hata ölçütü kullanılarak frekans bölgesinde yapılmaktadır.

Anahtar Kelimeler: Sualtı Akustik Kanal, Sönümlenen Kanallar, Kanal Simülasyonu, Değişken Optimizasyonu

To My Family

ACKNOWLEDGMENTS

I would like to express my deepest gratitude to my supervisor Assoc. Prof. Dr. Tolga ilođlu for his guidance, advice, criticism, encouragements and insight throughout the research.

Thanks to the examining committee members Prof. Dr. Mustafa Kuzuođlu, Assoc. Prof. Dr. ađatay Candan, Assoc. Prof. Dr. Ali zgür Yılmaz and Tevfik Bahadır Sarıkaya, Ms. Sc., for evaluating my work and for their valuable comments.

I would like to express my thanks especially to Mesude Civelekođlu, Oktay Sipahigil, Erdal Mehmetik, Berk Gürkakan and all my friends for their suggestions, support and fellowship.

Deepest thanks to my family for their love, trust, understanding, and every kind of support not only throughout my thesis but also throughout my life.

I would also like to thank Turkcell for their financial support during my graduate education.

TABLE OF CONTENTS

ABSTRACT	iv
ÖZ	v
ACKNOWLEDGMENTS	vii
TABLE OF CONTENTS	viii
LIST OF TABLES	x
LIST OF FIGURES	xi
CHAPTERS	
1 INTRODUCTION	1
1.1 Introduction	1
1.2 Outline	3
2 STATISTICAL MULTIPATH FADING CHANNEL MODELS	5
2.1 Introduction	5
2.2 Time-Varying Channel [1]	7
2.3 Narrowband Fading Model [1]	9
2.3.1 Autocorrelation, Cross Correlation and Power Spectral Density	13
2.3.2 Envelope and Power Distribution	17
2.4 Wideband Fading Model [1]	19
2.4.1 Power Delay Profile	24
2.4.2 Coherence Bandwidth	25
2.4.3 Doppler Power Spectrum and Channel Coherence Time	27
2.4.4 Transforms for Autocorrelation and Scattering Functions	28
3 UNDERWATER ACOUSTIC CHANNEL	30
3.1 The Ray Propagation Model [2]	31

3.2	Speed Of Sound [2]	32
3.2.1	Underwater Sound Channels	33
3.3	Attenuation and Noise	34
3.3.1	Spreading Loss	34
3.3.2	Absorption Loss	34
3.3.3	Ambient Noise	37
3.4	Multipath [2, 3, 4]	40
3.4.1	Micro- and Macro-Multipath	40
3.5	The Doppler Effect [3, 2]	44
3.6	Time Variability	47
4	SIMULATION OF UNDERWATER CHANNEL	49
4.1	Introduction	49
4.2	Ambient Noise Generation	51
4.3	Time Delay and Received Power	54
4.4	Doppler Spread and Doppler Power Spectrum	57
4.5	Loss	58
4.6	Multipath Formation and Micropath Effect	60
5	MODEL FITTING TO EXPERIMENTAL DATA	65
5.1	Introduction	65
5.2	Optimization of Channel Parameters	65
5.2.1	Optimizing the Sound Speed	65
5.2.2	Optimizing the Number of Paths	65
6	CONCLUSION	66
6.1	Results	66
6.2	Future Work	68
	REFERENCES	69

LIST OF TABLES

TABLES

Table 4.1	The physical conditions for Figure 4.7	55
Table 6.1	The scenarios for the planned measurement	68

LIST OF FIGURES

FIGURES

Figure 2.1	Multipath formation	6
Figure 2.2	Delay spread, T_m , for a single pulse input	10
Figure 2.3	Delay spread, T_m , input and output in narrowband fading model for a single symbol input	11
Figure 2.4	Formation of output signal given in bottom panel of Figure 2.3	11
Figure 2.5	Bessel Function versus $f_D\tau$	16
Figure 2.6	PSD of r_I and r_Q	17
Figure 2.7	Input signal consisting of two cascaded symbols	20
Figure 2.8	The output signal for narrowband fading model corresponding to input given in Figure 2.7	20
Figure 2.9	The output signal for wideband fading model corresponding to input given in Figure 2.7	21
Figure 2.10	Delay spread, T_m , input and corresponding output for wideband fading model	22
Figure 2.11	Power Delay Profile, RMS Delay and Coherence Bandwidth	27
Figure 2.12	Doppler Power Spectrum, Doppler Spread and Coherence Time	28
Figure 2.13	Fourier transform relations for $A_C(\Delta f; \Delta t)$, $A_c(\tau; \Delta t)$, $S_C(\Delta f; \rho)$ and $S_c(\tau; \rho)$	29
Figure 3.1	Reflection and refraction in shallow and deep water respectively	32
Figure 3.2	Speed profile in deep and shallow water	33
Figure 3.3	Attenuation of sound wave in sea water due to absorption	35
Figure 3.4	Average signal power with respect to range	37
Figure 3.5	Noise Power Spectral Density for <i>ship activity</i> =0 and <i>wind speed</i> =0, 5, 10 <i>m/s</i>	39

Figure 3.6	SNR depends on frequency and distance by the factor $1/A(r,f)N(f)$	39
Figure 3.7	Input delay spread function for a channel with five paths	43
Figure 3.8	Doppler effect for the case where the path between the transmitter and receiver increases due to relative motion during the propagation of the signal. Upper part belongs to transmitted signal whereas the lower part belongs to received signal for a single path only. 'a' is Doppler ratio	45
Figure 4.1	PSD relation between input and output of a filter	51
Figure 4.2	Underwater ambient noise generation by using white Gaussian noise	51
Figure 4.3	Theoretical and simulated underwater ambient noise Power Spectral Densities for wind speed=0 m/s	52
Figure 4.4	Time domain ambient noise signal	52
Figure 4.5	Spectrogram of ambient noise for wind speeds 0 and 10 m/s	53
Figure 4.6	Spectrogram of ambient noise for wind speeds 15 and 20 m/s	53
Figure 4.7	Received signals from different paths with different delay times; losses are ignored.	54
Figure 4.8	Received power and the received signal for 500 m horizontal distance	55
Figure 4.9	Received power and the received signal for 200 m horizontal distance	56
Figure 4.10	Relative times for 200m and 500m distances	56
Figure 4.11	Doppler shifts in the received signal, where the input frequency is 10KHz	57
Figure 4.12	Doppler power spectrum for a relative motion of +5m/s	58
Figure 4.13	Paths with spreading and absorption loss mechanisms only	60
Figure 4.14	Paths with all loss mechanisms	61
Figure 4.15	Random method multipath formation	62
Figure 4.16	Image method multipath formation	62
Figure 4.17	Micropath effect is seen on the paths. Note that there is no micropath effect on the first path	63
Figure 4.18	Micropath effect simulator	64

CHAPTER 1

INTRODUCTION

1.1 Introduction

Increasing interest in defense applications, off-shore oil industry, and other commercial operations in underwater environment provides underwater research to become more popular. Therefore in correlation to increase in interest, the number of research studies and applications that are conducted to explore underwater environment is increasing. In underwater environment, electromagnetic waves are subject to high attenuation and can only travel very short distances and therefore the only way that navigation, communication and other wireless applications can be done is through acoustic methods [5].

Underwater acoustic channel is difficult to work and has inherent problems. Difficulty comes from channel characteristics such as attenuation, multipath fading, time varying characteristics and inhomogeneities of the channel [6]. The attenuation in underwater channel is proportional to distance between the source and receiver and to square of the frequency of the signal, making the channel severely band limited[7]. Therefore underwater systems work at small frequencies, such as, on the order of tens of kHz . In addition to that, attenuation occurs due to reflections from bottom and surface of the channel.

In underwater channel multipaths occur due to reflections and refractions. Reflections generally occur from the bottom and the surface of the underwater channel whereas refractions occur due to sound channels created by the inhomogeneities of the sound speed. The number of multipaths reaching the receiver side can be very large, however the ones under noise level are ignored.

Internal and surface waves in an underwater channel continuously change the channel char-

acteristics by changing the reflection points of the transmitted signal. Moreover, the motion of these waves creates a Doppler effect in the channel. Underwater channel shows inhomogeneities in speed, temperature and salinity. The speed, temperature and salinity change as the depth of water changes. These variables may also change in time and may be different for the same depth of different places. Therefore, it can be said that the channel impulse response changes both spatially and temporarily. In addition to that as the place of the transmitter and receiver changes the channel impulse response also changes since the channel impulse response depends on the positions of the transmitter and receiver also.

Underwater channel is a double spread channel. It exhibits both dispersion in time (delay spread) and in frequency (Doppler spread) [7].

There are many of underwater channel models. Most of the channels implemented have used Ray theory as basis [8]. Galvin and Coates [9] have simulated the stochastic property of the channel (fading statistics) however they have not used physical properties of the underwater channel. The channel is implemented as tapped delayed sum of input, where the tap gains are complex random processes. This method was also used in [10].

The channel also has been described and simulated as a tapped delay line with variable delays, and stochastic tap gains in [11]. In addition to that, physical loss and Doppler factors are included using Bellhop acoustic toolbox [12].

In [13] the channel simulation contains physical properties of the channel, however the Doppler effect and micro-path effect is not included in simulation. The paths are formed by image method and with no randomness, therefore for the same number of paths under the same physical conditions the channel impulse response is found to be the same. In addition to that the surface, bottom and absorption loss are pre-determined which should be calculated according to depth, grazing angles and signal frequency.

In [14] the model is simulated using propagation loss and multipath fading properties. The Doppler effect and reflection loss parameters are not simulated.

In [15] multipath and micropath effects are implemented with loss delay and Doppler effect. The model in [15] is created using [16] and is physical based however there is no acoustical propagation physics mentioned such as spreading and absorption. In addition to that ambient noise has not been modeled. The formation of paths is random but multiple reflections are not

mentioned.

In [17] the physical properties of the underwater channel and multipath fading statistics are included. The model includes surface and bottom loss effects but they are taken to be constant for all cases where they should depend on the grazing angle and bottom type. Moreover the Doppler shift is not calculated but has been taken as a constant function of relative speed only where the sound speed should also be calculated and used to find Doppler shift.

In the model used for this thesis, nearly all physical properties of the underwater channel with multipath fading statistics have been used. The motion of the transmitter and emitter including the frequency spread due to motion of waves have been implemented. All types of the losses including grazing angles are also modeled. Moreover the ambient noise has also been modeled. Inhomogeneities of speed, temperature and salinity are included in the model.

The simulation is done in time domain using discrete data sampled at a sampling frequency of experiments conducted. However, analyses are done in both time and frequency domains. Furthermore the simulation outputs are observed and illustrated in both time and frequency domains.

1.2 Outline

The outline of this thesis is as follows: Chapter 2 gives a review about general multipath fading channel. Time varying characteristics of the channel are described by using a general channel impulse response for a multipath fading channel. Types of fading models and necessary conditions to obtain these types are presented. Characterization of channel according to these types using the channel impulse response and related functions are investigated. Definitions about a multipath fading channel and characterization functions and the relation between these functions are given.

In Chapter 3, physical properties of an underwater environment are given. Mathematical models of propagation loss, ambient noise, sound speed variation and ray propagation are presented. Channel impulse response, multipath models and Doppler effects specific to an underwater environment are explained.

The method and results of the simulations of the underwater channel model are presented

in Chapter 4. Time and frequency representations of the output of the channel for specific scenarios and input are investigated. The characterization functions *Power Delay Profile* and *Doppler Power Spectrum* obtained from these specific scenarios' outputs are discussed. The channel characteristic parameters, *Delay Spread* and *Doppler Spread* have been determined from these characterization functions.

In Chapter 5, the channel parameters are optimized and simulated channel impulse response is approximated to a real channel impulse response under specific scenarios. Undetermined parameters were *Sound Speed* and *the Number of Multipaths*. In Section 5.2.1 the sound speed is optimized by using a minimum mean square error criterion in frequency domain. Finally, in Section 5.2.2 the optimum number of paths for which the channel is best approximated is found for two specific scenarios. The approximation is illustrated by giving *Doppler Power Spectra* of the simulated and the real channel before and after optimization.

Conclusions and future work are given in Chapter 6.

CHAPTER 2

STATISTICAL MULTIPATH FADING CHANNEL MODELS

2.1 Introduction

Underwater channels are multipath fading channels therefore investigation of underwater channel will be started with studying multipath fading channels. In this chapter a general multipath fading channel will be considered. *Multipath channel* and *fading* phenomenon will be defined and necessary conditions and assumptions for different types of fading will be given. Some important parameters that are related to multipath fading communication channels and that will be mentioned in this thesis are as follows:

Multipath Propagation: In a wireless communication system, due to reflections caused by environmental conditions, natural and man-made objects through the channel and due to channel characteristics, multiple of transmitted signals are obtained at receiver side. Figure 2.1 shows a multipath formation for a wireless channel.

Fading: In multipath propagation, all paths having different amplitude, delay, phase shift and frequency shift are added on the receiver side, in this addition the signal amplitude can severely decrease or increase. This phenomenon is called *multipath fading* [18]

Delay: The transmitted signal reaches the receiver after some time during propagation due to fact that propagation speed of the transmitted signal is not infinite.

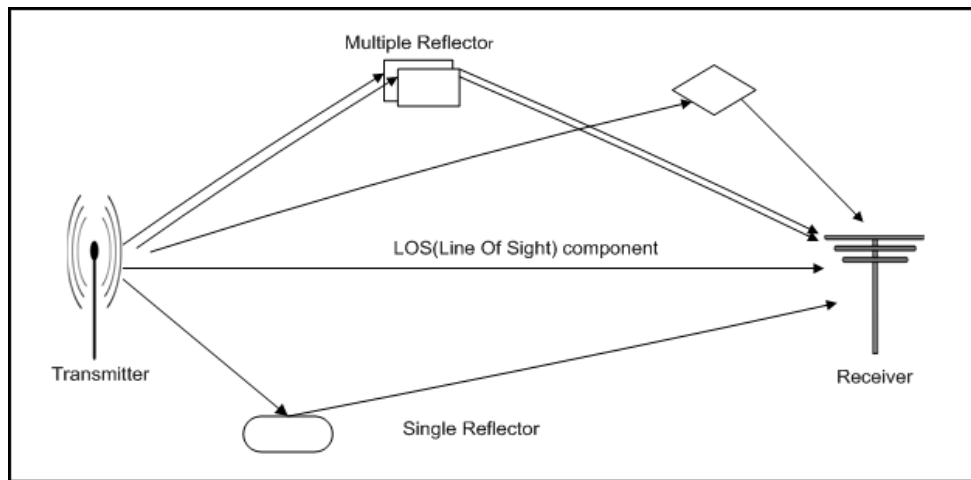


Figure 2.1: Multipath formation

Doppler Effect: Due to relative motion between the transmitter and receiver or due to motion of reflection point of the transmitted signal, frequency and phase shift are observed at the receiver side.

Delay Spread: In a multipath channel the time difference between the last arrival path over noise level and synchronized path is called Delay Spread. In another words, if the first arrival is taken as synchronized path, Delay Spread is called maximum delay after which the received signal is under noise level. Figure 2.2 shows delay spread for a situation where the first arrival is taken as synchronized multipath component.

Power Delay Profile: Gives average power of a signal received through a multipath channel as a function of multipath delay.

Doppler Power Spectrum: Gives Power Spectral Density (PSD) of the received signal as a function of Doppler frequency(shift).

Doppler Spread: It is described as the range of frequencies over which Doppler power spectrum is non-zero. Doppler spread gives information about spectral broadening due to channel characteristics.

Coherence Time: It is the time over which it can be accepted that the channel impulse response is nearly the same. It is proportional to the inverse of *Doppler Spread*.

Coherence Bandwidth: It is the bandwidth over which the channel frequency response can be accepted to be essentially invariant. It is inversely proportional to *Delay Spread*.

Attenuation: The energy of the transmitted signal is not completely transferred to the receiver side. Some part of the energy is transferred to the heat energy. In addition to that all transmitted energy does not reach the receiver but other sides.

In a multipath channel, for each single pulse transmitted, a pulse train with LOS (Line Of Sight) and/or distinct multipath components will appear on the receiver side. There are two important characteristics of a multipath channel: time delay spread and time varying nature[1]. The characteristics of a multipath fading channel will be discussed in more detail in the following sections.

2.2 Time-Varying Channel [1]

Time variation of channel is due to relative motion between the transmitter and receiver or change of reflection points of multipaths in the channel [1]. In wireless channels, time variation is nearly inevitable since there are factors that cannot be controlled and change continuously. In order to understand the time variation better let the transmitted signal for a time varying channel be as follows:

$$s(t) = \mathcal{R}\{u(t)e^{j2\pi f_c t}\} = \mathcal{R}\{u(t)\} \cos(2\pi f_c t) - \mathcal{I}\{u(t)\} \sin(2\pi f_c t), \quad (2.1)$$

then the received signal for multipath time varying channel will be as follows:

$$r(t) = \mathcal{R}\left\{\sum_{n=0}^{N(t)} \alpha_n(t) u(t - \tau_n(t)) e^{j(2\pi f_c(t - \tau_n(t)) + \phi_{D_n(t)})}\right\}. \quad (2.2)$$

In (2.1) and (2.2) $u(t)$ is the complex envelope of the transmitted signal $s(t)$ with bandwidth B_u and f_c is the carrier frequency (Bandwidth of a signal is taken as approximately inverse of

its symbol duration i.e. $B \approx 1/T_s$ where T_s is symbol duration). In (2.2), the received signal $r(t)$ is the combination of LOS component ($n = 0$) and other delayed multipath components. In (2.2), $N(t)$, $\alpha_n(t)$, $\tau_n(t)$ and $\phi_{D_n}(t)$ are the number of resolvable multipath components, amplitude of the n^{th} component, corresponding delay and Doppler phase shift, respectively.

Two multipath components with delays τ_n and τ_m are resolvable if $|\tau_n - \tau_m| \gg 1/(B_u)$ otherwise they are unresolvable since $u(t - \tau_n) \approx u(t - \tau_m)$. Each n^{th} path given in (2.2) may be reflected from a single reflector or multiple reflectors clustered together as shown in Figure 2.1.

In case of multiple reflectors the delay of the multipaths will be very close and are combined to be a single multipath component with rapidly varying amplitude due to constructive and destructive addition of multipath components causing non resolvable paths. Generally wide-band channels have resolvable multipath components, however, narrowband channels have non resolvable multipath components.

In (2.2) the received signal can be simplified by letting

$$\phi_n(t) = 2\pi f_c \tau_n(t) - \phi_{D_n}(t), \quad (2.3)$$

then $r(t)$ becomes as follows:

$$r(t) = \mathcal{R}\left\{\left[\sum_{n=0}^{N(t)} \alpha_n(t) e^{-j\phi_n(t)} u(t - \tau_n(t))\right] e^{j2\pi f_c t}\right\}. \quad (2.4)$$

The amplitude $\alpha_n(t)$ depends on loss and shadowing and $\phi_n(t)$ depends on delay and Doppler. Therefore $\alpha_n(t)$ and $\phi_n(t)$ can be accepted as independent random processes. They are characterized as random process since they change over time.

The received signal can be represented as the convolution of the baseband input signal $u(t)$ and time-varying impulse response $c(\tau, t)$ and followed by up conversion with carrier frequency f_c :

$$r(t) = \mathcal{R}\left\{\left(\int_{-\infty}^{\infty} c(\tau, t) u(t - \tau) d\tau\right) e^{j2\pi f_c t}\right\} \quad (2.5)$$

Here $c(\tau, t)$ is the channel impulse response and has two variables: t is the time that the corresponding impulse is received and $t - \tau$ is the time that the impulse is sent.

When (2.4) and (2.5) are compared, $c(\tau, t)$ is obtained as follows:

$$c(\tau, t) = \sum_{n=0}^{N(t)} \alpha_n(t) e^{-j\phi_n(t)} \delta(\tau - \tau_n(t)). \quad (2.6)$$

In some cases, in the channel there can be continuum of multipath delays then the sum in (2.6) becomes an integral so $c(\tau, t)$ becomes as follows (time-varying complex amplitude associated with each delay τ):

$$c(\tau, t) = \int \alpha(\xi, t) e^{-j\phi(\xi, t)} \delta(\tau - \xi) = \alpha(\tau, t) e^{-j\phi(\tau, t)}. \quad (2.7)$$

In the following sections this impulse response, $c(\tau, t)$, will be used to characterize the channel model.

Fading model can be defined according to relationship between delay spread, T_m and signal bandwidth, B . If the spread of time delays associated to LOS and all other components is smaller than the inverse of signal bandwidth ($T_m \ll B^{-1}$) then components are non resolvable (narrowband fading model), otherwise the components are resolvable (wideband fading model) these cases will be discussed in more detail in Section 2.3 and 2.4 respectively. Delay spread can be measured in different ways but the important point is the choice of component to which receiver is synchronized, say here it is τ_x , then the delay spread is calculated as $T_m = \max_n |\tau_n - \tau_x|$. For a single pulse input, the delay spread T_m is shown in Figure 2.2. Here it should be noted that there are infinite number of multipath components but the one whose power has gone under noise level should not contribute to the delay spread. It is obvious that the multipath delays vary in the time so T_m becomes a random variable.

2.3 Narrowband Fading Model [1]

As discussed in Section 2.2 when $T_m \ll B^{-1}$, that is when delay spread is smaller than bandwidth of the signal, narrowband fading model is obtained. In this case $u(t - \tau_i) \approx u(t)$ since $\tau_i \leq T_m \forall i$, then (2.4) becomes as follows:

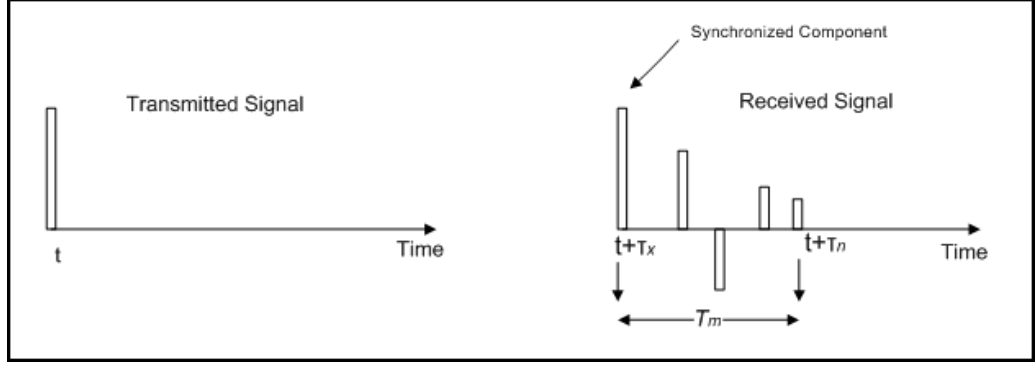


Figure 2.2: Delay spread, T_m , for a single pulse input

$$r(t) = \mathcal{R}\left\{u(t)e^{j2\pi f_c t}\left(\sum_n \alpha_n(t)e^{-j\phi_n(t)}\right)\right\}. \quad (2.8)$$

The situation where $T_m \ll B^{-1}$ is satisfied can be illustrated for a single transmitted symbol; a symbol of duration 0.1 s and delay spread of 0.01 s, the input and related output obtained for a multipath fading channel is shown in Figure 2.3. In the top panel, the transmitted symbol and in the middle panel, the symbol up converted with carrier frequency are given. The middle plot is the input signal given to the multipath fading channel. The bottom panel shows the output of the multipath fading channel. The signal's duration is extended by the delay spread. The amplitude, phase and frequency of the signal have changed since the channel output is combination of different multipath components with random amplitudes, phases and frequencies. Figure 2.4 shows the simulation conducted to form the output signal given in bottom panel of Figure 2.3.

In Figure 2.4 n is the number of multipaths, input and output signals are middle and bottom panels of Figure 2.3 respectively. τ_m is the random delay for the m^{th} path and it is in the interval $[\tau_{first}, \tau_{first}+T_m]$, where T_m is delay spread and it is 0.01 for this case and τ_{first} is the delay of the first arrival and in this case it is direct path and it is equivalent to τ_1 . In order to obtain a narrowband fading model the maximum difference between last and first arrival is assured to be smaller than predetermined delay spread. α_m is the random loss for the m^{th} path and assuming the SNR is 20 dB, it is smaller than 20 dB. f_m and θ_m are random frequency and phase shifts for the m^{th} path. f_m is smaller than maximum frequency that can be obtained from Doppler effect resulted from the relative motion between the transmitter and receiver. θ_m

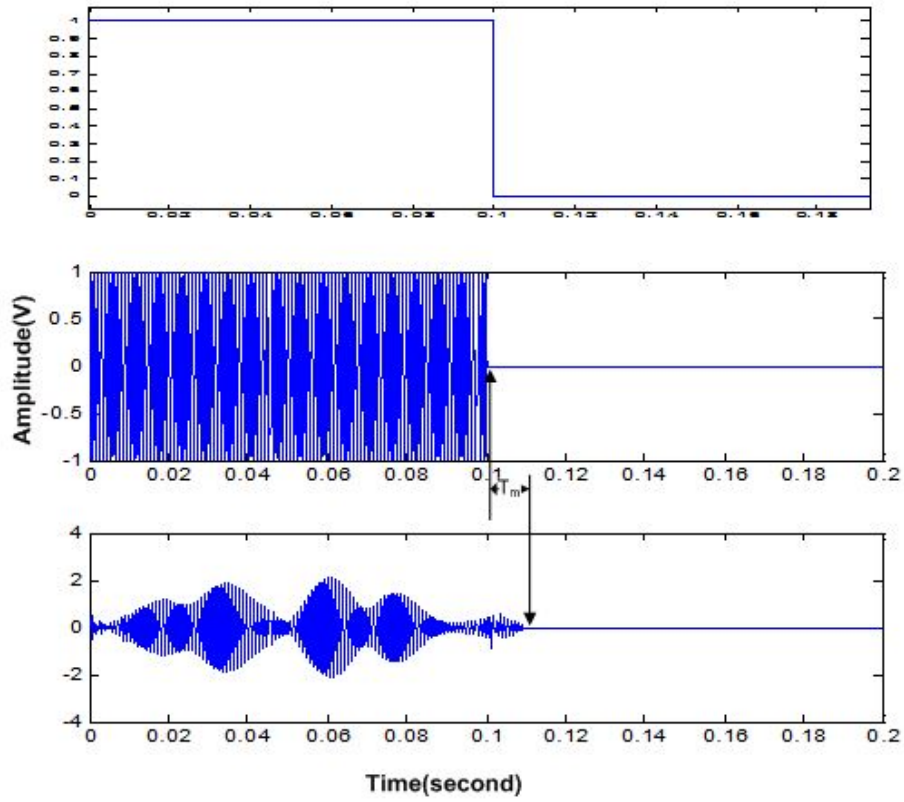


Figure 2.3: Delay spread, T_m , input and output in narrowband fading model for a single symbol input

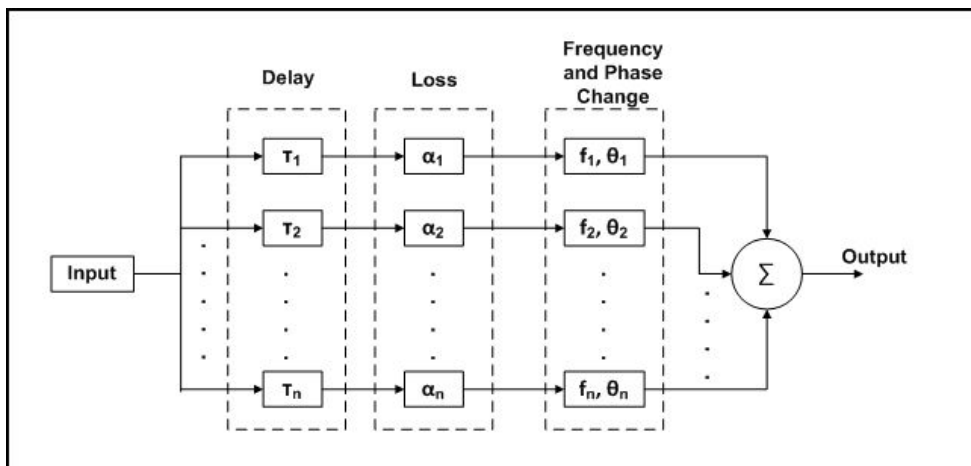


Figure 2.4: Formation of output signal given in bottom panel of Figure 2.3

is randomly chosen from the interval $[0, \pi]$. Note that the values of loss, frequency and phase shift are not so critical in this simulation. The aim is to obtain a narrowband fading model by assuring the $T_m \ll B^{-1}$ condition, therefore the critical parameters are delay spread and symbol duration. Note also that in bottom panel of Figure 2.3 the time axis is relative to the receiver side, that is the first arrival time is taken as starting time.

When (2.8) is compared to (2.1), it is seen that the only difference is the complex scale factor $\left(\sum_n \alpha_n(t)e^{-j\phi_n(t)}\right)$ and this factor is independent from baseband signal $u(t)$ or equivalently from the transmitted signal $s(t)$. In order to describe the random scale factor resulted from multipath, $s(t)$ is chosen as an unmodulated carrier with phase ϕ_0 which is narrowband for any T_m :

$$s(t) = \mathcal{R}\{e^{j2\pi f_c t + \phi_0}\} = \cos(2\pi f_c t - \phi_0). \quad (2.9)$$

Then by this assumption the received signal becomes as follows:

$$r(t) = \mathcal{R}\left\{\left[\sum_{n=0}^{N(t)} \alpha_n(t)e^{-j\phi_n(t)}\right]e^{j2\pi f_c t}\right\} = r_I(t)\cos(2\pi f_c t) + r_Q(t)\sin(2\pi f_c t), \quad (2.10)$$

where in-phase and quadrature components $r_I(t)$ and $r_Q(t)$ are as follows:

$$r_I(t) = \sum_{n=1}^{N(t)} \alpha_n(t)\cos(\phi_n(t)), \quad (2.11)$$

$$r_Q(t) = \sum_{n=1}^{N(t)} \alpha_n(t)\sin(\phi_n(t)), \quad (2.12)$$

and the phase term $\phi_n(t)$ is as follows:

$$\phi_n(t) = 2\pi f_c \tau_n(t) - \phi_{D_n} - \phi_0. \quad (2.13)$$

It is seen in (2.13) that the phase term contains the phase offset ϕ_0 and the effects of delay and Doppler.

In case of large $N(t)$, by using Central Limit Theorem and the fact that $\alpha_n(t)$ and $\phi_n(t)$ are stationary and ergodic, it can be shown that $r_I(t)$ and $r_Q(t)$ can be approximated to be jointly Gaussian. In case of small $N(t)$, the Gaussian property still holds if $\alpha_n(t)$ are Rayleigh distributed and $\phi_n(t)$ are uniformly distributed on $[-\pi, \pi]$ [1].

2.3.1 Autocorrelation, Cross Correlation and Power Spectral Density

In this section autocorrelation and cross-correlation functions of the in-phase and quadrature components, $r_I(t)$ and $r_Q(t)$, of the received signal are derived. In the derivation, some basic assumptions are made, these assumptions are applicable in the case of absence of a dominant LOS component. In this section it is assumed that the variables; amplitude $\alpha_n(t)$, multipath delay $\tau_n(t)$ and Doppler frequency $f_{D_N}(t)$ change slowly enough over the interested time interval that they are assumed to be constant, that is $\alpha_n(t) \approx \alpha$, $\tau_n(t) \approx \tau$ and $f_{D_N}(t) \approx f_{D_N}$. Under this assumption the Doppler phase shift and phase of the n th term become as $\phi_{D_n}(t) = \int_t 2\pi f_{D_n} dt = 2\pi f_{D_n} t$ and $\phi_n(t) = 2\pi f_c \tau_n - 2\pi f_{D_n} t - \phi_0$ respectively.

The next assumption which is a key and a reasonable assumption is that the term $2\pi f_c \tau_n$ for the n th term changes more rapidly than other terms in the phase. This is because of the fact that f_c is large and for a small change in τ_n , $2\pi f_c \tau_n$ can go through a 360 degree rotation. Therefore the phase term is assumed to be uniformly distributed over $[-\pi, \pi]$. With these assumptions we get the expected value of the in-phase part of the received signal as follows:

$$E[r_I(t)] = E\left[\sum_n \alpha_n \cos\phi_n(t)\right] = \sum_n E[\alpha_n] E[\cos\phi_n(t)] = 0. \quad (2.14)$$

Note that in (2.14) the second equality comes from independence of α_n and ϕ_n and last equality comes from uniform distribution of ϕ_n around zero. Similarly it can be shown that $E[r_Q(t)] = 0$. Hence the received signal has also zero-mean, $E[r(t)] = 0$, and since $r_I(t)$ and $r_Q(t)$ are jointly Gaussian the received signal is zero-mean Gaussian. Note that these mean values are valid in the case when there is no dominant LOS component in the received signal. If there is a LOS component, the received signal's phase is affected by the phase of LOS component and random uniform phase assumption is no longer valid.

The autocorrelation of in-phase and quadrature components using independency of α_n and ϕ_n and independence of ϕ_n and ϕ_m , $n \neq m$, can be obtained as follows:

$$\begin{aligned}
E[r_I(t)r_Q(t)] &= \left[\sum_n \alpha_n \cos\phi_n(t) \sum_m \alpha_m \sin\phi_m(t) \right] \\
&= 0.
\end{aligned} \tag{2.15}$$

This shows that $r_I(t)$ and $r_Q(t)$ are uncorrelated and since they are jointly Gaussian process, they are independent. In a similar way as in (2.15) the autocorrelation of $r_I(t)$ is obtained as follows:

$$A_{r_I}(t, \tau) = E[r_I(t)r_I(t + \tau)] = \sum_n E[\alpha_n^2] E[\cos\phi_n(t)\cos\phi_n(t + \tau)]. \tag{2.16}$$

Making the substitution $\phi_n(t) = 2\pi f_c \tau_n - 2\pi f_{D_n} t - \phi_0$ and considering the fact that $4\pi f_c \tau_n$ term changes more rapidly than other terms and since it is uniformly distributed (2.16) reduces to

$$A_{r_I}(t, \tau) = 1/2 \sum_n E[\alpha_n^2] E[\cos(2\pi f_{D_n} \tau)] = 1/2 \sum_n E[\alpha_n^2] \cos(2\pi v \tau \cos\theta_n / \lambda), \tag{2.17}$$

since $f_{D_n} = v \cos\theta_n / \lambda$ where $\lambda = c / f_c$. Note that $A_{r_I}(t, \tau)$ depends only on τ , that is $A_{r_I}(t, \tau) = A_{r_I}(\tau)$ therefore $r_I(t)$ is wide-sense stationary (WSS) random process. Similarly it can be shown that quadrature component $r_Q(t)$ is also WSS with autocorrelation function $A_{r_I}(\tau) = A_{r_Q}(\tau)$. Moreover the cross-correlation between in-phase and quadrature components also depends only on τ and it is given as follows:

$$\begin{aligned}
A_{r_I, r_Q}(t, \tau) &= A_{r_I, r_Q}(\tau) = E[r_I(t)r_Q(t + \tau)] \\
&= -0.5 \sum_n E[\alpha_n^2] \sin(2\pi v \tau \cos\theta_n / \lambda) \\
&= -E[r_Q(t)r_I(t + \tau)].
\end{aligned} \tag{2.18}$$

Using (2.17) and (2.18) it can be shown that the received signal $r(t)$ is also WSS with autocorrelation function

$$A_r(\tau) = E[r(t)r(t + \tau)] = A_{r_I}(\tau) \cos(2\pi f_c \tau) + A_{r_I r_Q}(\tau) \sin(2\pi f_c \tau) \tag{2.19}$$

To simplify equations (2.18) and (2.17) a model called uniform scattering environment is used [1]. In this model, it is assumed that each multipath component has an angle of arrival $\theta_n = n\Delta\theta$ where $\Delta\theta = 2\pi/N$. Moreover it is assumed that each multipath component has the same received power that is $E[\alpha_n^2] = 2P_r/N$ where P_r is the total received power.

Considering these assumptions and making the substitution $N = 2\pi/\Delta\theta$ (2.17) becomes

$$A_{r_I} = \frac{P_r}{2\pi} \sum_{n=1}^N \cos(2\pi\nu\tau \cos n\Delta\theta/\lambda)\Delta\theta \quad (2.20)$$

Assuming infinite number of multipaths ($N \rightarrow \infty, \Delta\theta \rightarrow 0$) with uniform scattering the summation in (2.20) becomes an integral:

$$A_{r_I} = \frac{P_r}{2\pi} \int \cos(2\pi\nu\tau \cos\theta/\lambda)d\theta = P_r J_0(2\pi f_D\tau), \quad (2.21)$$

where

$$J_0(x) = \frac{1}{\pi} \int_0^\pi e^{-jx\cos\theta} d\theta \quad (2.22)$$

is a Bessel function of the 0th order. Its plot with respect to $f_D\tau$ is given in Figure 2.5. Similarly under this uniform scattering assumption the cross correlation between in-phase and quadrature components becomes as follows:

$$A_{r_I, r_Q}(\tau) = \frac{P_r}{2\pi} \int \sin(2\pi\nu\tau \cos\theta/\lambda)d\theta = 0. \quad (2.23)$$

In Figure 2.5, it is seen that the autocorrelation is zero for $f_D\tau \approx 0.4$ or equivalently $\nu\tau \approx 0.4\lambda$. Therefore it can be said that over an approximately half wavelength distance the signal decorrelates, under uniform scattering assumption made previously. Another interesting property seen in Figure 2.5 is that the signal recorreates after it becomes uncorrelated.

The power spectral densities(PSDs) of received in-phase and quadrature components, r_I and r_Q are obtained by computing the Fourier transforms of their autocorrelation functions and are given as follows:

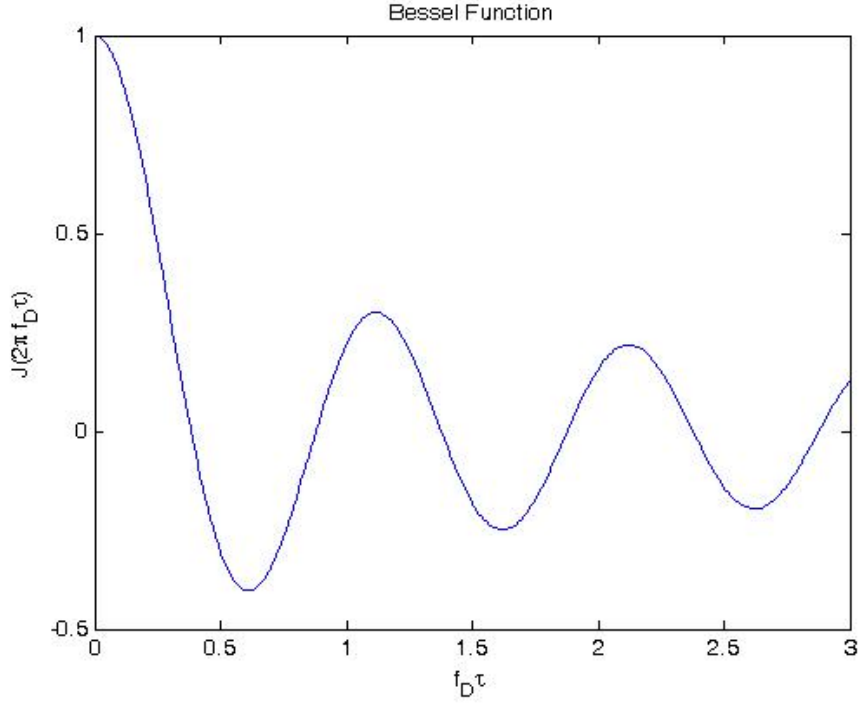


Figure 2.5: Bessel Function versus $f_D\tau$

$$S_{r_I}(f) = S_{r_Q}(f) = \mathcal{F}[A_{r_I}(\tau)] = \begin{cases} \frac{P_r}{2\pi f_D} \frac{1}{\sqrt{1-(f/f_D)^2}} & |f| \leq f_D \\ 0 & \text{else} \end{cases} \quad (2.24)$$

PSD given in (2.24) is shown in Figure 2.6. Note that the plot given in Figure 2.6 is the Fourier transform of the plot given in Figure 2.5 with scale factor P_r , since $A_{r_I} = P_r J_0(2\pi f_D\tau)$.

To obtain PSD of the received signal under uniform scattering assumption, (2.19) with $A_{r_I r_Q} = 0$ will be used. Therefore PSD of the received signal is obtained as follows:

$$\begin{aligned} S_r(f) &= \mathcal{F}[A_r(\tau)] = 0.25[S_{r_I}(f - f_c) + S_{r_I}(f + f_c)] \\ &= \begin{cases} \frac{P_r}{4\pi f_D} \frac{1}{\sqrt{1-(\frac{f-f_c}{f_D})^2}} & |f - f_c| \leq f_D \\ 0 & \text{else.} \end{cases} \end{aligned} \quad (2.25)$$

Note that the integral of PSD of the received signal is equal to total received power, P_r .

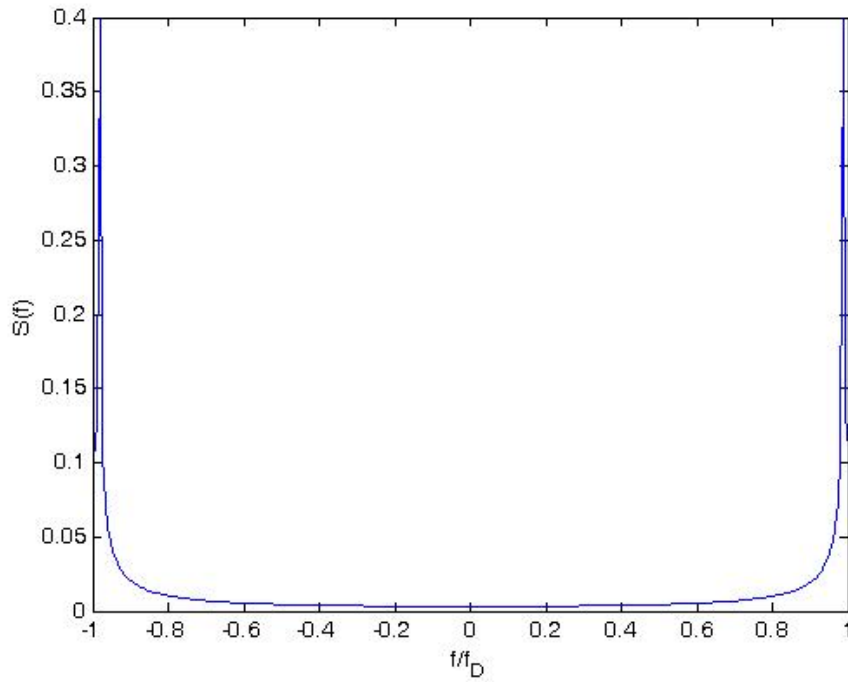


Figure 2.6: PSD of r_I and r_Q

The PSD given in (2.25) models the power spectral density related to multipaths as a function of Doppler frequency. Therefore it can be seen as distribution of random frequency due to Doppler. It is seen that the PSD of in-phase and quadrature components goes to infinity at $f = \pm f_D$ and PSD of the received signal goes to infinity at $f = \pm f_c \pm f_D$, in practice this is not true since uniform scattering is just an approximation. However, they take their maximum values at these points. PSDs are useful in simulation of fading process. Commonly, for simulating envelope of the narrowband fading process two independent white Gaussian noise process with $PSD = N_0/2$ are filtered through low pass filters with frequency response $H(f)$ such that $S_{r_I}(f) = S_{r_Q}(f) = \frac{N_0}{2}H(f)$ is satisfied. The output of the filters are then in-phase and quadrature components of narrowband fading process.

2.3.2 Envelope and Power Distribution

The distribution of the envelope of the received signal in fading channel gives information about the type of fading channel and therefore physical characteristics of the fading channel. For uniform distribution assumption, r_I and r_Q are both zero-mean Gaussian random

variables. It is known that for two random variables X and Y , $Z = \sqrt{X^2 + Y^2}$ is Rayleigh distributed if X and Y are Gaussian random variables with mean zero and equal variance σ^2 and moreover Z^2 is exponentially distributed. Therefore the envelope of the received signal, $r(t)$, say $z(t) = |r(t)|$ is Rayleigh distributed

$$p_Z(z) = \frac{2z}{P_r} \exp[-z^2/P_r] = \frac{z}{\sigma^2} \exp[-z^2/(2\sigma^2)], \quad z \geq 0, \quad (2.26)$$

where $P_r = \sum_n E[\alpha_n^2] = 2\sigma^2$ is the average received power of the signal. The power distribution can be obtained by making change of variables $z^2(t) = |r(t)|^2$ in (2.26). Thus

$$p_{Z^2}(x) = \frac{1}{P_r} e^{-x/P_r} = \frac{1}{2\sigma^2} e^{-x/(2\sigma^2)}, \quad x \geq 0, \quad (2.27)$$

will be the power distribution of the signal. Note that the received signal power has exponential distribution with mean $2\sigma^2$. The complex low pass equivalent of $r(t)$ is given by $r_{LP}(t) = r_I(t) + jr_Q(t)$. The phase of the $r_{LP}(t)$ is given by $\theta = \arctan(r_Q(t)/r_I(t))$, when $r_I(t)$ and $r_Q(t)$ are uncorrelated Gaussian random variables, θ is uniformly distributed and independent of r_{LP} .

The envelope distribution and power distribution given in (2.26) and (2.27) are valid in the case where there is no significant LOS component. If there is a significant LOS component in the channel then $r_I(t)$ and $r_Q(t)$ are not zero mean and the received signal is superposition of complex Gaussian component and LOS component. In this case the envelope of the received signal will have Rician distribution

$$p_Z(z) = \frac{z}{\sigma^2} \exp\left[-\frac{(z^2 + s^2)}{2\sigma^2}\right] I_0\left(\frac{zs}{\sigma^2}\right), \quad z \geq 0. \quad (2.28)$$

In (2.28) $2\sigma^2 = \sum_{n,n \neq 0} E[\alpha_n^2]$ is the average power of the received multipath components except LOS component and $s^2 = \alpha_0^2$ is the power of LOS component, I_0 is modified Bessel function of order zero. Therefore the average received power in Rician fading is $P_r = s^2 + 2\sigma^2$. The Rician distribution is generally characterized by a fading parameter which is given by $K = \frac{s^2}{2\sigma^2}$ that is the ratio of power in the LOS component to the ratio of power in other multipath components. Note that when $K = 0$, no LOS component case, Rayleigh distribution is obtained and when $K = \infty$ there is no fading, that is there is no multipath component.

Both Rician and Rayleigh distributions can be used in modeling physical properties of the fading channels. However, their results do not fit to some experimental data therefore a more general and practical fading distribution is necessary to fit experimental data. For this purpose Nakagami fading distribution [1] which is given in (2.29) was developed.

$$p_Z(z) = \frac{2m^m z^{2m-1}}{\Gamma(m)P_r^m} \exp\left[-\frac{mz^2}{P_r}\right], \quad m \geq 0.5, \quad (2.29)$$

where P_r is the average received power and $\Gamma(\cdot)$ is Gamma function. Note that for $m = 1$ the Nakagami distribution reduces to Rayleigh fading and for $m = (K+1)^2/(2K+1)$ approximates to Rician fading with fading parameter K . Moreover when $m = \infty$ there is no fading.

2.4 Wideband Fading Model [1]

In a multipath channel even if the signal is not narrowband distortion occurs due to multipath delay spread, T_m . In this case, a transmitted pulse of duration T will be received in a longer duration of $T+T_m$, that is the duration of the received signal will increase as much as multipath delay spread, T_m .

When $T_m \ll T$ time spreading is small however due to fact that in the receiving side multipath components associated with the same transmitted pulse are obtained on top of one another, destructive and constructive interference occurs. This is shown in Figure 2.8. The signal obtained in Figure 2.8 is output of the multipath fading channel where the input is given in Figure 2.7. In Figure 2.7 at the upper side the two symbols that will be transmitted are given and at lower side the symbols up converted by carrier frequency are given. Figure 2.8 is obtained using the narrowband fading model described in Section 2.3. The outputs of both symbols given in bottom panel of Figure 2.7 are obtained separately and they are drawn on top of each other.

In Figure 2.8 the destructive and constructive effects of multipaths are easily seen. Furthermore it is seen that the amplitude, phase and frequency of the signal has been hugely changed. In addition to these it is seen that Inter Symbol Interference(ISI) is small since delay spread is small compared to symbol durations.

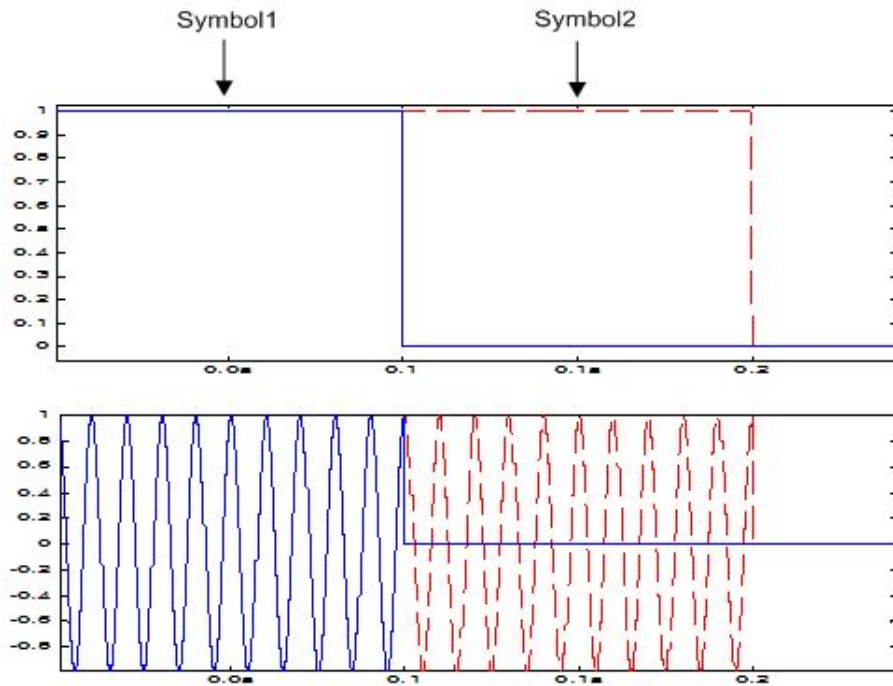


Figure 2.7: Input signal consisting of two cascaded symbols

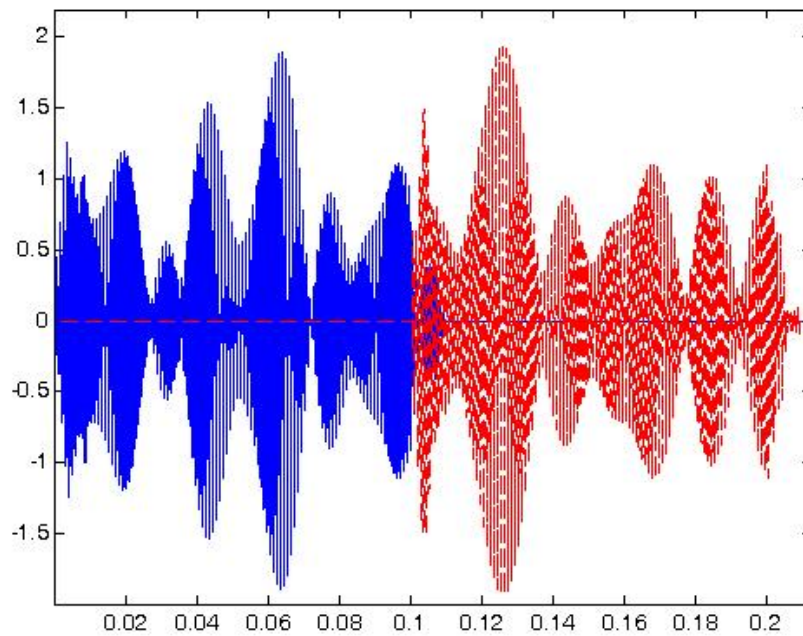


Figure 2.8: The output signal for narrowband fading model corresponding to input given in Figure 2.7

However when $T_m \gg T$ each multipath component associated with the same transmitted pulse can be resolved, but in this case multipath components interfere with subsequently transmitted pulses resulting in Inter Symbol Interference (ISI). This is shown in Figure 2.9. In Figure 2.9 it is seen that the delay spread is so large that the multipath components corresponding to two different components are obtained on the top of one another at the receiving side. That is the ISI is large. Moreover it is also seen that the multipath components corresponding to the same input symbol are resolvable however they are obtained on the top of another multipath component corresponding another input symbol. Even the multipath components corresponding to the same input symbol are resolvable still destructive and constructive effects are seen due to fact that some multipath components have the same or close multipath delays. Therefore the amplitude, phase and frequency are again disturbed.

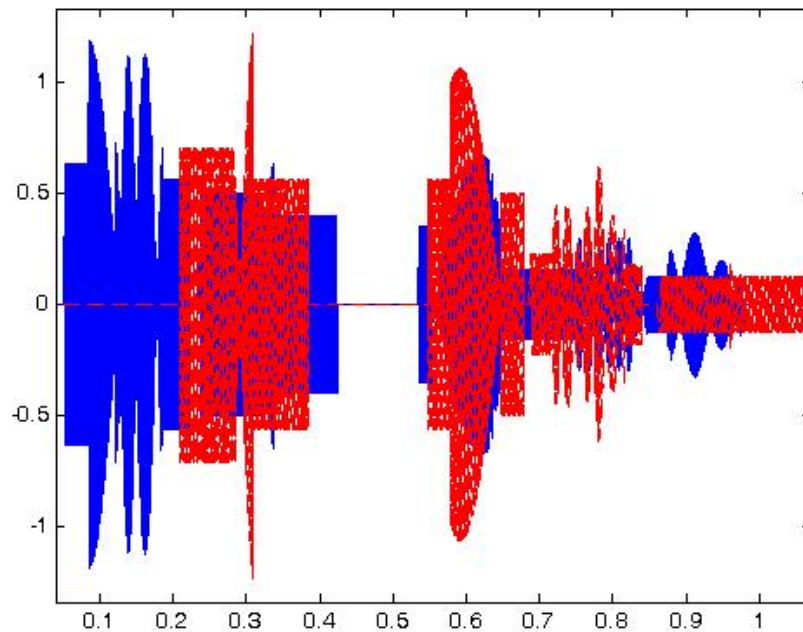


Figure 2.9: The output signal for wideband fading model corresponding to input given in Figure 2.7

In Section 2.3 it is stated that when $T_m \ll B^{-1}$ narrowband fading model is obtained, where B is the bandwidth of the signal. However, in wideband fading model $T_M \gg B^{-1}$ and the approximation $u(t - \tau_n(t)) \approx u(t)$ is no longer valid. Therefore, the received signal is sum of delayed and shifted copies of the transmitted signal. Each copy will have its own delay τ_n

and phase $\phi_n(t)$ values. When the phase terms are large, the copies will combine destructively causing distortions in the received signal. An example of wideband fading model with symbol duration 0.1 s and delay spread of 1 s is given in Figure 2.10.

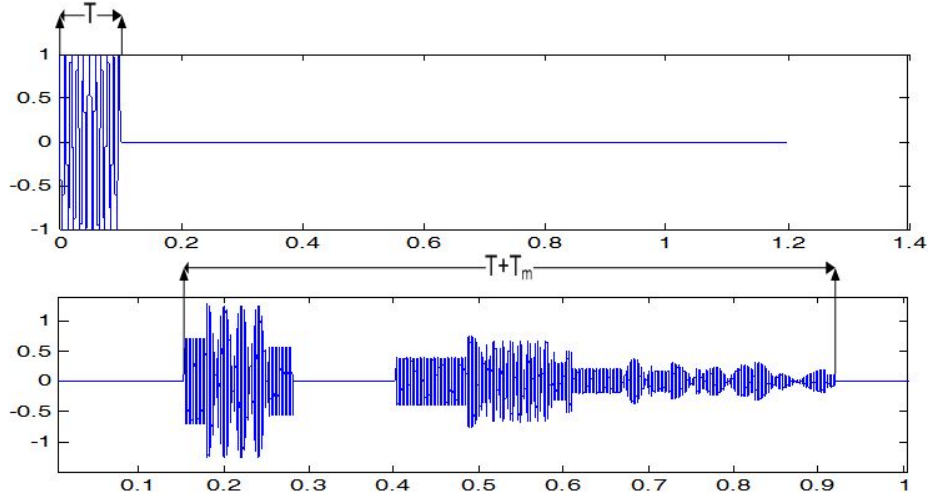


Figure 2.10: Delay spread, T_m , input and corresponding output for wideband fading model

Figure 2.10 is obtained using Figure 2.4. However, in this case the delay spread is taken as 1 s where the symbol duration is the same.

Gaussianity property holds in wideband fading model if the number of multipath components is large and phase of each component is uniformly distributed. Then the received signal will be zero-mean complex Gaussian process with Rayleigh distributed envelope as in narrowband fading model. Despite this, wideband fading is different from narrowband fading. Difference is seen in the resolution of different multipath components. In narrowband fading the signal at the receiver can be identified just by its amplitude and phase which are characterized by random processes. These random processes are described by their autocorrelation or PSD and their instantaneous distributions. Nevertheless, wideband fading cannot be identified just by amplitude and phase random processes since the received signal has distortions occurred due to delay spread of different multipath components. Therefore in wideband fading, both multipath delay spread and time variations of the channel should be considered as effects of multipath phenomenon.

In order to identify wideband fading channel, low-pass equivalent impulse response, $c(\tau, t)$,

will be investigated. Assuming the impulse response, $c(\tau, t)$, as deterministic function of τ and t , its Fourier transform with respect to t is obtained as follows:

$$S_c(\tau, \rho) = \int_{-\infty}^{\infty} c(\tau, t) e^{-j2\pi\rho t} dt. \quad (2.30)$$

$S_c(\tau, \rho)$ is called **deterministic scattering function** of the low-pass equivalent of the channel impulse response. Since $S_c(\tau, \rho)$ is Fourier transform of $c(\tau, t)$ with respect to time, it gives information about Doppler characteristic of the channel by the frequency parameter ρ .

The time-varying channel impulse response $c(\tau, t)$ given in (2.6) is generally random not deterministic, since the multipath components have random amplitude, phase, delay and number of multipath components. So it is characterized statistically. As it was mentioned above if there are enough number of multipath components $c(\tau, t)$ can be assumed to be complex Gaussian process. Therefore, its statistical properties can be completely determined by its mean, autocorrelation and cross-correlation of in-phase and quadrature components. It is assumed that each multipath component has uniformly distributed phase as in narrowband fading model. Therefore in-phase and quadrature components of $c(\tau, t)$ are independent Gaussian processes with the same autocorrelation, mean of zero and cross-correlation of zero. If the number of multipath components are small the same characteristics are still true if each multipath component has Rayleigh distributed amplitude and uniformly distributed phase. This model holds when there is not a dominant LOS component.

The autocorrelation function of $c(\tau, t)$, which gives its statistical properties is given as follows:

$$A_c(\tau_1, \tau_2; t, \Delta t) = E[c^*(\tau_1; t)c(\tau_2; t + \Delta t)]. \quad (2.31)$$

Here it is assumed that the channel is WSS, that is the autocorrelation function is independent of time, t , but depends on time difference Δt . Joint statistic measured at two different times depends on time difference (in practice most channels are WSS). Thus, (2.31) becomes as follows:

$$A_c(\tau_1, \tau_2; \Delta t) = E[c^*(\tau_1; t)c(\tau_2; t + \Delta t)]. \quad (2.32)$$

In practice the channel response corresponding to multipath component of delay τ_1 is uncorrelated with channel response corresponding to multipath component with different delay τ_2 , where $\tau_1 \neq \tau_2$. This is because they are scattered by different scatterers. Such a channel has uncorrelated scattering (US). Channels which are both WSS and US are abbreviated as WSSUS. When US property is included in (2.32), it yields

$$E[c^*(\tau_1; t)c(\tau_2; t + \Delta t)] = A_c(\tau_1; \Delta t)\delta[\tau_1 - \tau_2] \triangleq A_c(\tau; \Delta t). \quad (2.33)$$

$A_c(\tau; \Delta t)$ given in (2.33) is the average output power corresponding to channel as a function of multipath delay $\tau = \tau_1 = \tau_2$ and time difference Δt in observation time. For this function it is assumed that delay difference is bigger than inverse of bandwidth that is, $|\tau_1 - \tau_2| > B^{-1}$, in order to resolve two components.

The **scattering function** for random channels is Fourier transform of $A_c(\tau; \Delta t)$ with respect to Δt and is given as follows:

$$S_c(\tau, \rho) = \int_{-\infty}^{\infty} A_c(\tau, \Delta t)e^{-j2\pi\rho\Delta t} d\Delta t. \quad (2.34)$$

$S_c(\tau, \rho)$ identifies average power corresponding to channel as a function of multipath delay τ and Doppler ρ since it is Fourier transform of $A_c(\tau, \Delta t)$. The most important properties of the wideband channel is obtained from autocorrelation function $A_c(\tau, \Delta t)$ or scattering function $S_c(\tau, \rho)$.

2.4.1 Power Delay Profile

Power delay profile $A_c(\tau)$, also called multipath intensity profile is defined as $A_c(\tau) \triangleq A_c(\tau, 0)$. It is obvious that power delay profile gives average power associated with a given multipath delay.

If the pdf of random delay spread T_m is defined in terms of $A_c(\tau)$ as follows:

$$p_{T_m} = \frac{A_c(\tau)}{\int_0^{\infty} A_c(\tau) d\tau}, \quad (2.35)$$

then mean and rms delay spread are defined as follows:

$$\mu_{T_m} = \frac{\int_0^{\infty} \tau A_c(\tau) d\tau}{\int_0^{\infty} A_c(\tau) d\tau} \quad (2.36)$$

$$\sigma_{T_m} = \sqrt{\frac{\int_0^{\infty} (\tau - \mu_{T_m})^2 A_c(\tau) d\tau}{\int_0^{\infty} A_c(\tau) d\tau}} \quad (2.37)$$

where μ_{T_m} and σ_{T_m} are mean and rms delay spreads respectively. Defining mean, rms delay spread or equivalently pdf given in (2.35) in terms of $A_c(\tau)$ means that the delay associated with a given multipath component is related to its power. Therefore the multipath components with small power contributes less to delay spread. In general the multipath components which are below noise floor are not used for calculation of multipath delay spread.

In general a delay T where $A_c(\tau) \approx 0$ for $\tau \geq T$ can be used for the delay spread of the channel and this value is taken as integer multiple of rms delay spread, that is $T = 3\sigma_{T_m}$. Under this approximation, $A_c(\tau) \approx 0$ for $\tau > 3\sigma_{T_m}$, a linearly modulated signal with symbol period T_s can have or not have ISI depending on the relation between T_s and σ_{T_m} . If $T_s \ll \sigma_{T_m}$ (wideband fading) then the signal will experience a large ISI. In contrast if $T_s \gg \sigma_{T_m}$ (narrowband fading) then the signal will experience negligible ISI. Finally when T_s is on the order of σ_{T_m} then there will be some ISI which may or may not decrease the performance of the system depending on the properties of the system and channel.

The relationship between μ_{T_m} and σ_{T_m} depends on the shape of $A_c(\tau)$, but in general $\mu_{T_m} \approx \sigma_{T_m}$. If there is no LOS component and small number of multipath components with nearly the same delays in the channel then $\mu_{T_m} \gg \sigma_{T_m}$.

2.4.2 Coherence Bandwidth

Time varying multipath random channel can also be characterized by taking Fourier transform of the channel impulse response $c(\tau, t)$ with respect to τ , that is it will be investigated in the frequency domain. Thus,

$$C(f; t) = \int_{-\infty}^{\infty} c(\tau, t) e^{-j2\pi f\tau} d\tau. \quad (2.38)$$

It is known that $c(\tau, t)$ is WSS and is a complex zero-mean Gaussian random variable in t , therefore $C(f; t)$ is also WSS and zero-mean complex Gaussian random process since it is the integral of $c(\tau, t)$ and (2.38) represents the sum of complex zero-mean Gaussian processes. Therefore $C(f; t)$ can be characterized by its autocorrelation function which is given as:

$$A_C(f_1, f_2; \Delta t) = E[C^*(f_1; t)C(f_2; t + \Delta t)]. \quad (2.39)$$

$A_C(f_1, f_2; \Delta t)$ can be simplified as follows :

$$\begin{aligned} A_C(f_1, f_2; \Delta t) &= E\left[\int_{-\infty}^{\infty} c^*(\tau_1; t)e^{j2\pi f_1 \tau_1} d\tau_1 \int_{-\infty}^{\infty} c(\tau_2; t + \Delta t)e^{-j2\pi f_2 \tau_2} d\tau_2\right] \\ &= A_C(\Delta f; \Delta t), \end{aligned} \quad (2.40)$$

where $\Delta f = f_1 - f_2$ and the equality is obtained by the help of WSS and US property of $c(\tau; t)$.

If Δt is taken zero in (2.40) then Fourier transform of the power delay profile, $A_c(\tau)$ is obtained which is defined as $A_C(\Delta f) \triangleq A_C(\Delta f; 0)$ and is given as follows

$$A_C(\Delta f) = \int_{-\infty}^{\infty} A_c(\tau)e^{-j2\pi f \tau} d\tau. \quad (2.41)$$

$A_C(\Delta f)$ can also be shown to be $A_C(\Delta f) = E[C^*(f; t)C(f + \Delta f; t)]$, that is it is an autocorrelation function. Then the channel response is independent at approximately Δf frequency separations where $A_C(\Delta f) \approx 0$. The frequency B_c is called the **coherence bandwidth** of the channel where $A_C(\Delta f) \approx 0$ for all $\Delta f > B_c$. By the Fourier transform relation it is obvious that when $A_c(\tau) \approx 0$ for $\tau > T$ then $A_C(\Delta f) \approx 0$ for $\Delta f > 1/T$. Therefore, the coherence bandwidth B_c can be approximated as $B_c \approx 1/T$, where T is generally taken as *RMS* delay spread, σ_{T_m} , of $A_c(\tau)$. A more general approximation can be made as $B_c \approx k/\sigma_{T_m}$ where k depends on the shape of $A_c(\tau)$ and exact definition of coherence bandwidth.

According to the signal bandwidth transmitted, the fading can be **flat (frequency non-selective)** or **frequency-selective**. If the bandwidth of the transmitted signal B is $B \ll B_c$ then the fading is nearly equal for all signal bandwidth, that is it is highly correlated. In this case flat fading is obtained. In linear modulation the signal bandwidth is inversely proportional to

symbol time T_s . Therefore for flat fading it means that $T_s \approx 1/B \gg 1/B_c = \sigma_{T_m}$, that is there is negligible ISI in the channel. Conversely if B is $B \gg B_c$ then frequency selective fading is obtained. In this case the channel amplitude through the signal bandwidth is highly changing this is because the channel amplitude value at frequencies separated more than coherence bandwidth are roughly independent. In frequency selective fading $T_s \approx 1/B \ll 1/B_c = \sigma_{T_m}$, that is there is large ISI in the channel. A plot of $A_c(\tau)$ and its Fourier transform $A_C(\Delta f)$ with two signals which are narrowband and wideband signals is given in Figure 2.11.

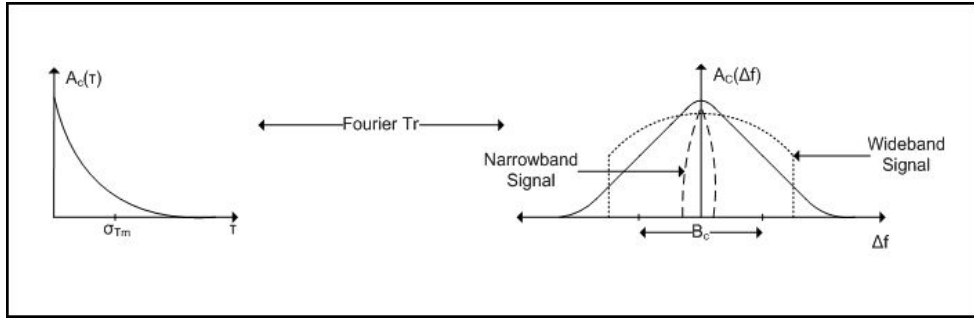


Figure 2.11: Power Delay Profile, RMS Delay and Coherence Bandwidth

In Figure 2.11 it is seen that $A_C(\Delta f)$ is flat across narrowband signal whereas widely changing across wideband signal. Frequency selectivity is also seen from Figure 2.11, since fading is different and independent for different parts of the wideband signal.

2.4.3 Doppler Power Spectrum and Channel Coherence Time

Due to motions of receiver or transmitter time variations occur in the channel. These time variations cause Doppler shifts in the received signal. This Doppler effect can be investigated by taking the Fourier transform of the autocorrelation function $A_C(\Delta f; \Delta t)$ with respect to Δt :

$$S_C(\Delta f; \rho) = \int_{-\infty}^{\infty} A_C(\Delta f; \Delta t) e^{-j2\pi\rho\Delta t} d\Delta t \quad (2.42)$$

In order to identify Doppler at a single frequency Δf can be taken as zero. Then (2.42) becomes as follows:

$$S_C(\rho) = \int_{-\infty}^{\infty} A_C(\Delta t) e^{-j2\pi\rho\Delta t} d\Delta t, \quad (2.43)$$

where $A_C(\Delta t) \triangleq A_C(\Delta f = 0; \Delta t)$ is the autocorrelation function which gives information about how channel impulse response decorrelates over time.

Specifically, when $A_C(\Delta t = T) = 0$ is satisfied, observations of the channel impulse response separated by T are uncorrelated and so independent since the channel impulse response is Gaussian random process. **Channel coherence time**, T_c is defined to be the range over which $A_C(\Delta t)$ is nonzero. Therefore it can be said that time varying channel decorrelates after approximately T_c seconds. $S_C(\rho)$ given in (2.43) is called Doppler power spectrum of the channel and gives PSD of the received signal as a function of Doppler ρ , since it is Fourier transform of autocorrelation function $A_C(\Delta t)$. The maximum ρ value for which $S_C(\rho)$ is approximately nonzero is called Doppler spread and is shown by B_D . Using the Fourier transform relationship between $A_C(\Delta t)$ and $S_C(\rho)$, it is obtained that $B_D \approx 1/T_c$. In general $B_D \approx k/T_c$ where k depends on the shape of $S_C(\rho)$. A plot of Doppler power spectrum and its inverse Fourier transform is given in Figure 2.12.

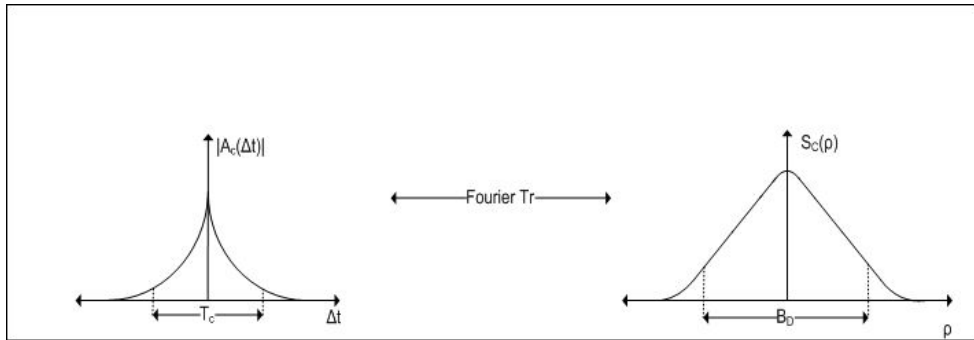


Figure 2.12: Doppler Power Spectrum, Doppler Spread and Coherence Time

2.4.4 Transforms for Autocorrelation and Scattering Functions

The four functions $A_C(\Delta f; \Delta t)$, $A_c(\tau; \Delta t)$, $S_C(\Delta f; \rho)$ and $S_c(\tau; \rho)$ obtained until now are related to each other with Fourier transforms with respect to each other. The relationships between these four functions are given in Figure 2.13.

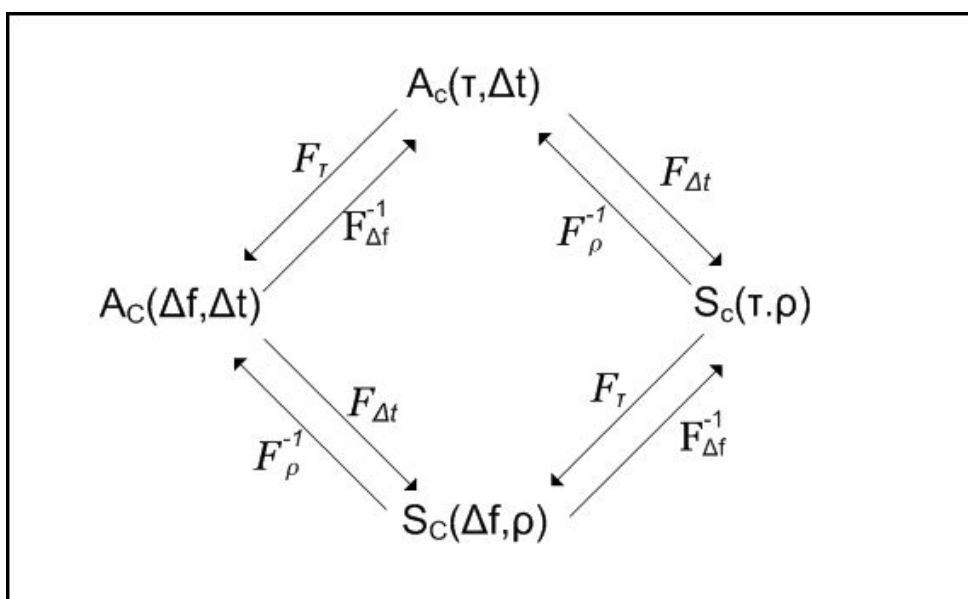


Figure 2.13: Fourier transform relations for $A_C(\Delta f; \Delta t)$, $A_C(\tau; \Delta t)$, $S_C(\Delta f; \rho)$ and $S_C(\tau; \rho)$

CHAPTER 3

UNDERWATER ACOUSTIC CHANNEL

The channel model given in Chapter 2 is a general multipath fading channel for electromagnetic waves in air. Underwater acoustic channel (UAC) can also be modeled as a multipath fading channel. However, there is not a standardized model proposed for underwater acoustic channel fading for the moment and experimental studies are conducted to determine the statistical properties of underwater acoustic channel [4]. There are basic differences in between wireless channels in air and in underwater. The attenuation increases as frequency increases in underwater channels. The existence of surface and bottom layers limits the propagation of acoustic signals and greatly increases the multipath effects. The rapid fluctuations resulted from surface waves decreases coherence time of underwater channel. The speed of the acoustic signal in underwater environment is smaller compared to electromagnetic signals in air and it is comparable with the speed of the receiver and the transmitter . Therefore, the Doppler effect is larger in underwater channels.

Underwater acoustic channel (UAC) is one of the most difficult channels for data transmission, communication and signal processing. Difficulty of the media comes from its complex, dynamic and unpredictable nature. Underwater channel may quickly change by environmental and biological conditions. The underwater channel's behavior is best characterized with extremely unpredictable and varying multipath, very large propagation delays, attenuation of signals increasing with distance and frequency, low and limited bandwidth, time variable physical conditions, noise, low and varying speed of sound, high Doppler spread, time varying Doppler shift and ambient interference. These phenomena can significantly damage signal as it propagates through the channel. Therefore in order to get a reliable channel model for underwater signal processing the factors mentioned above should be accounted for. The prop-

agation of an acoustic signal in underwater channel is best succeeded in low frequencies due to the fact that the attenuation of the acoustic signal increases as its frequency increases. The bandwidth of the channel is severely limited and is distance dependent. Although the bandwidth is low, underwater systems are actually wideband since the bandwidth of the channel is not negligible compared to center frequency. In underwater channel the received signal has greater bandwidth and time duration than transmitted signal, such channels are called spread channels. Spread channels can be represented by a time-varying impulse response $c(\tau, t)$ [11] where t is time and τ is delay.

3.1 The Ray Propagation Model [2]

The acoustic waves in the ocean generally can be assumed as propagating through rays or paths at frequencies greater than $5kHz$. This assumption is valid when the inhomogeneities are larger than the wavelength of the waves in spatial scale. The speed of sound in the ocean is around $1500m/s$ therefore for the frequencies assumption made the wavelength is less than $1/3$ meter. The speed of sound depends on depth, temperature and salinity of the water and therefore varies significantly while propagating under water. According to Snell's law spatial variability causes bending of rays; rays of sound waves bend towards the lower speed region [4]. This is referred to as refraction. In addition to these refraction rays the wave also propagates through the rays which are reflected from surface and bottom of the sea. Both of the factors *refraction* and *reflection* are shown in Figure 3.1. Note that for refraction to occur there must be a change of speed of sound during propagation which generally occurs in deep water. On the other side, reflections generally occur in shallow water.

The rays and paths mentioned above can be defined by the equations (3.1) and (3.2).

$$\frac{d\theta}{dx} = c(z)^{-1} \frac{dc(z)}{dz} \quad (3.1)$$

$$\frac{dz}{dx} = -\tan(\theta(x)) \quad (3.2)$$

where x , z and θ are as shown in Figure 3.1 and are horizontal distance, depth and angle with respect to the horizontal, respectively. The speed of the sound, $c(z)$, varies vertically faster

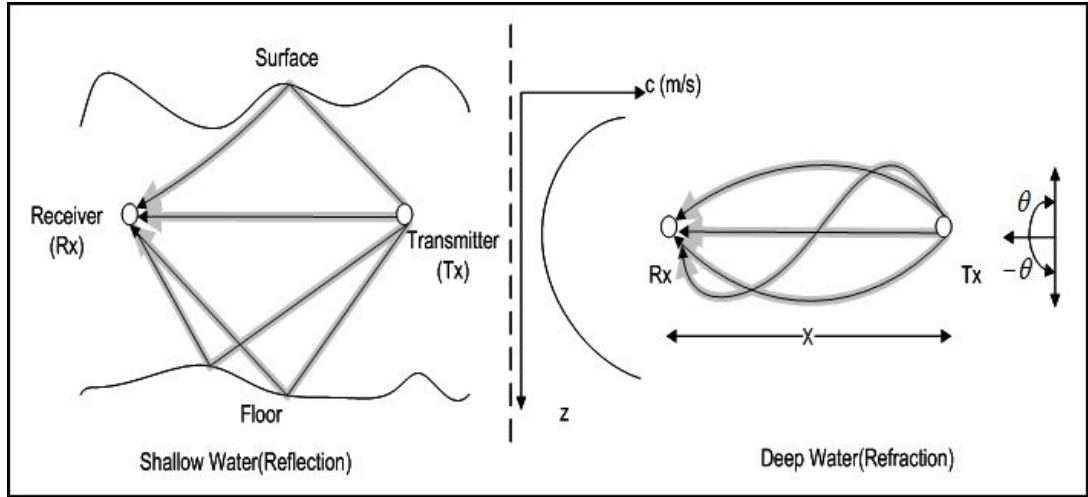


Figure 3.1: Reflection and refraction in shallow and deep water respectively

than it varies horizontally.

3.2 Speed Of Sound [2]

The speed of sound in underwater environment depends on temperature, depth and salinity of the water. Therefore the speed of sound shows spatial and temporal variabilities. This is because of the fact that the water is not homogeneous in temperature and salinity and as depth changes hydrostatic pressure changes. The speed of sound in the sea is approximated as follows [19]:

$$c(T, S, z) = 1449.2 + 4.6T - 0.055T^2 + 0.00029T^3 + (1.34 - 0.01T)(S - 35) + 0.016z \quad (3.3)$$

where c is speed of sound and T , S and z are temperature (in degrees), salinity (in parts per thousand) and depth (in meters) respectively. At the regions near the surface the temperature and pressure are generally constant and therefore so is the sound speed. As the depth increases the temperature decreases and the sound speed also decreases even though the pressure increases; the effect of temperature dominates on the sound speed. After some depth, the temperature becomes constant ($4^\circ C$) and from that point on, the sound speed starts to increase due to pressure increase. Sound speed shows different profiles in deep and shallow water due to different environmental conditions. These profiles are shown in Figure 3.2.

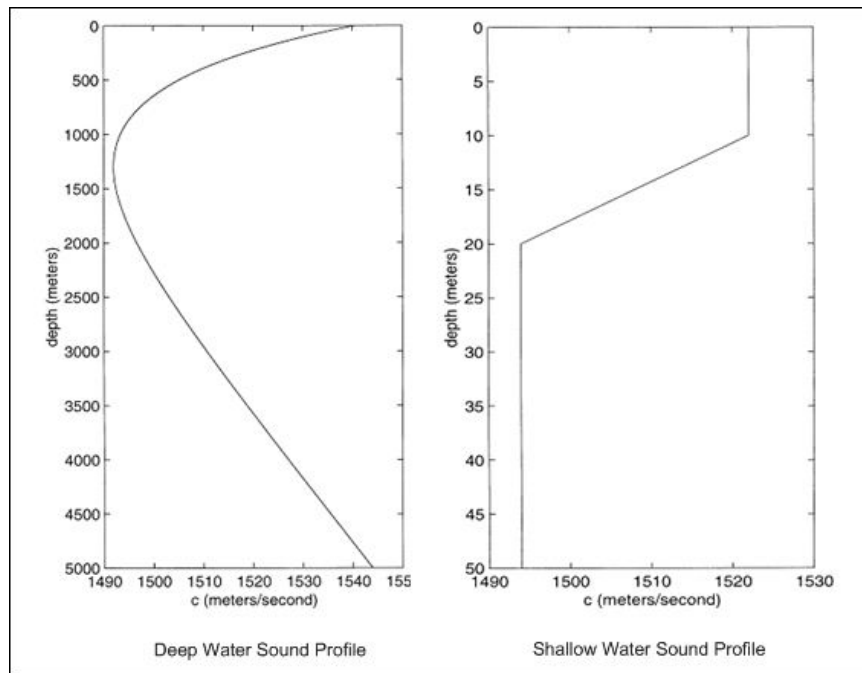


Figure 3.2: Speed profile in deep and shallow water

3.2.1 Underwater Sound Channels

As it is seen in Figure 3.2, in deep water, at mid-attitudes there exists a channel in which the speed of the sound becomes minimum. The sound tends to bend towards the low speed regions therefore if a speed wave propagates along this channel it will be trapped in this channel, in another words a natural waveguide occurs. This region or channel in which the sound rays are trapped is called sound channel or SOFAR channel.

In shallow water, there also exists SOFAR channels but they are different from the deep water SOFAR channels in the sense that they may not exists always since the temperature of the shallow water greatly changes with seasonal changes therefore the sound speed profile may be different for different seasons. The SOFAR channel in the shallow water is also called surface sound channel.

3.3 Attenuation and Noise

In an underwater acoustic channel, the energy of the transmitted signal is partly transferred to heat energy. In addition to that some parts of the energy is lost during scatterings from the surface and bottom. In an underwater acoustic channel the loss mechanisms are spreading loss, absorption loss and scattering loss.

3.3.1 Spreading Loss

The spreading loss is seen in two types; spherical loss for deep water and cylindrical loss for shallow water [20]. Actually, the spherical and cylindrical loss is categorized according to the distance from the source point. If the vertical propagation has reached to its limit imposed by sea floor and sea surface then from that point on cylindrical propagation starts for horizontal propagation. In spherical loss the attenuation of the signal is proportional to inverse square of the distance from source point ($1/r^2$, where r is distance from the source) and for cylindrical loss it is proportional to inverse of distance from the source point ($1/r$). Therefore the spreading loss for a distance r from source point is given by (3.4).

$$L_s = r^k \quad (3.4)$$

In (3.4), k is energy spreading factor and it is 2 for spherical, 1 for cylindrical and 1.5 for practical spreading [21].

3.3.2 Absorption Loss

In an acoustic channel one of the most important distinguishing property is the fact that the path loss depends on signal's frequency. The reason for that fact is the transfer of acoustic energy to the heat energy, that is absorption loss. Absorption loss can be approximated as follows:

$$L_a = a^f \quad (3.5)$$

where r is the distance from the source point and a is the frequency dependent term which is given as [21]:

$$a = 10^{\alpha(f)/10} \quad (3.6)$$

The term $\alpha(f)$ in (3.6) is the absorption coefficient [19]:

$$\alpha(f) = 0.11 \frac{f^2}{1 + f^2} + 44 \frac{f^2}{4100 + f^2} + 2.75(10^{-4} f^2) + 0.003 \quad (3.7)$$

The attenuation coefficient is in dB/km and f is in kHz . The attenuation coefficient as a function of frequency is shown in Figure 3.3.

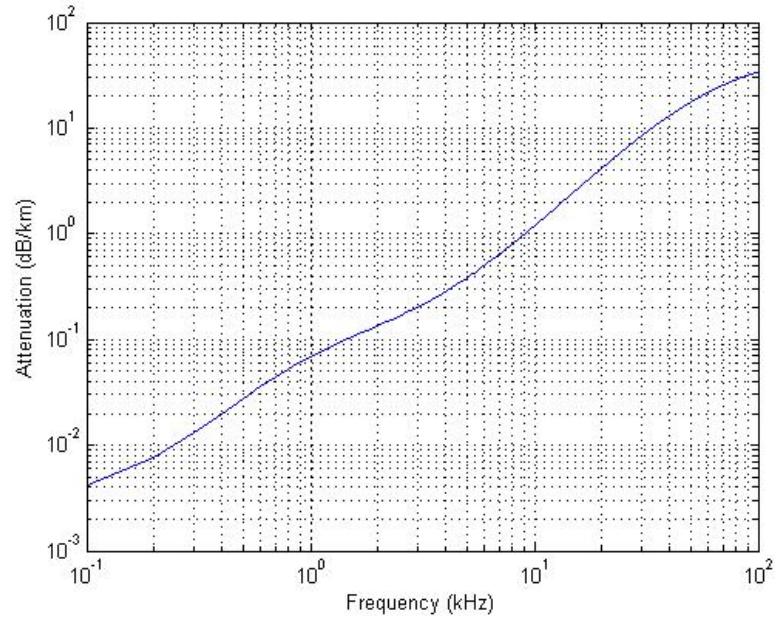


Figure 3.3: Attenuation of sound wave in sea water due to absorption

In addition to the spreading and absorption losses there is a loss because of the interaction of sound wave with sea surface and sea floor, that is scattering loss. If the sea surface and sea floor is rough then most of the sound signal scatters to the directions different from receiver's direction causing loss of energy in the signal. In addition to this some part of the sound signal penetrates through the bottom and some of it does not reflect from the sea surface and passes through the surface causing more signal losses. The signal loss due to penetration into

the bottom is greatly higher than absorption through the water. The loss due to surface and bottom scattering increases as grazing angle of the sound increases. Moreover, for bottom scattering case the loss greatly depends on the type of the bottom.

In deep water, existence of SOFAR channel causes the sound wave to propagate without interacting with bottom and surface. This decreases the amount of loss and therefore increases the amount of distance that the sound wave can travel. In SOFAR channel, the only sources of loss are spreading and absorption loss by the water. Therefore it can be said that the effective range over which sound can travel is larger in deep water than that in shallow water.

Ignoring the loss due to interaction with surface and bottom, scattering loss and fading effect due to multipath, the signal level (SL in dB) at a distance r from the source can be obtained as follows [2]:

$$SL = 169 + 10\log_{10}(P) - \alpha r - 20\log_{10}(d/2) - 10\log_{10}(r - d/2) \quad (3.8)$$

where P is the power of the radiated signal in watts, α is the absorption coefficient, r is the distance from the source point and d is the depth of the water and the constant term 169 comes from conversion of electric power to acoustic power. In (3.8) it is assumed that the transducer is omni-directional and the depth of the water is smaller than the distance from the source, that is $d < r$. Moreover, the first two terms in (3.8) are due to signal power, the other terms are due to absorption loss, spherical loss and cylindrical loss respectively. Note that here the total loss is the combination of spreading loss and absorption loss which is given as:

$$A(r, f) = (r)^k a(f)^r \quad (3.9)$$

where r , k and f are the distance from the transmitter, energy spreading factor and frequency, respectively. The average signal power with respect to range for the depths 50m, 100m and 150m is given in Figure 3.4.

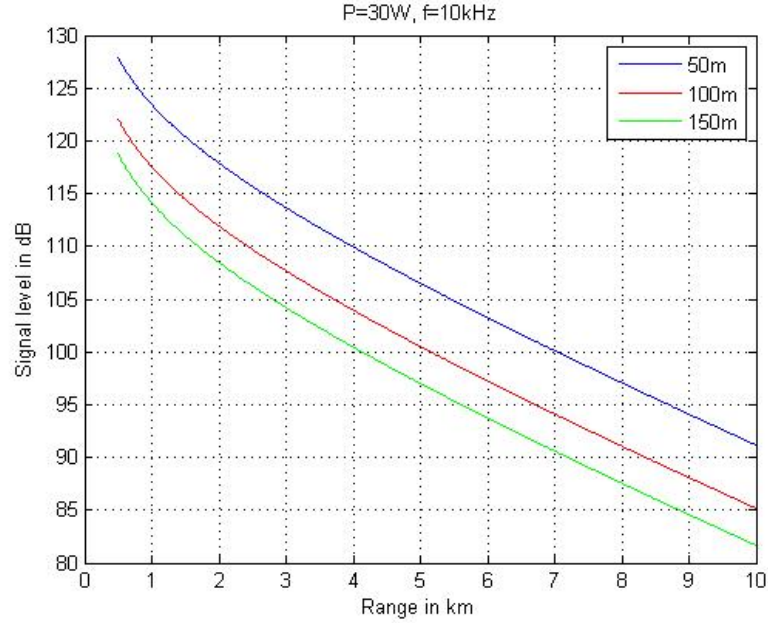


Figure 3.4: Average signal power with respect to range

3.3.3 Ambient Noise

In addition to these losses there is noise which also should be accounted for in underwater systems. The noise is strongly dependent on frequency and site of underwater channel [22]. There are many sources of noise in underwater channel such as turbulence, marine life, breaking waves, passing ships, rain, winds and man-made noise. The noise in underwater acoustic channel can be classified as ambient noise and site-specific noise. The ambient noise is always present as contrary to the site specific noise. The ambient noise has a continuous spectrum and Gaussian statistics (but not white since it is frequency dependent) and it is assumed that its power spectral density decays with about $20dB/decade$ [22]. On the other side, site-specific noise often can have significant non-Gaussian components. Therefore it can be said that the nature of noise depends on its source. Due to man-made noises, the noise in seaside environments is generally higher than the noise in deep water. The amplitude of the total noise can be different from time to time for a certain location and certain frequency due to variability of the environment.

Underwater ambient noise is composed of many sources. Main components of these sources are wind, temperature, turbulence and shipping activity [23]. The noise factors for $N_w(\text{wind})$,

N_{te} (temperature), N_{tu} (turbulence) and N_s (shipping activity) are given in dB re μPa as follows:

$$10\log_{10}(N_w(f)) = 50 + 7.5w^{0.5} + 20\log_{10}(f) - 40\log_{10}(f + 0.4) \text{ dB re } \mu Pa \quad (3.10)$$

$$10\log_{10}(N_{te}(f)) = -15 + 20\log_{10}(f) \text{ dB re } \mu Pa \quad (3.11)$$

$$10\log_{10}(N_{tu}(f)) = 17 - 30\log_{10}(f) \text{ dB re } \mu Pa \quad (3.12)$$

$$10\log_{10}(N_s(f)) = 40 + 20(s - 0.5) + 26\log_{10}(f) - 60\log_{10}(f + 0.03) \text{ dB re } \mu Pa \quad (3.13)$$

where w is wind speed in m/s , s is the shipping activity and f is in kHz . The shipping activity lies between 0(no activity) and 1(maximum activity). The *re* abbreviation given in units of noises given in (3.13) stands for *relative*. Therefore, the values of noises given in (3.13) are relative to $1\mu Pa$ in dB scale. The total ambient noise is obtained as

$$N(f) = N_w(f) + N_{te}(f) + N_{tu}(f) + N_s(f). \quad (3.14)$$

The power spectral density of the total noise given in (3.14) is shown in Figure 3.5. The most important factor of the total noise in the range $100Hz < f < 100kHz$ is the wind speed. This range is usually operating region for most of the underwater acoustic systems.

As it is mentioned above the attenuation increases as frequency increases and as the propagation range increases. Therefore the SNR on the receiver side is a function of frequency and range [4]. SNR on the receiver side is given as follows:

$$SNR(r, f) = S_t(f)/(A(r, f)N(f)) \quad (3.15)$$

where $S_t(f)$ is power spectral density of the transmitted signal. In (3.15) it is seen that SNR depends on $1/A(r, f)N(f)$ factor which is shown in Figure 3.6.

In Figure 3.6 it is seen that the bandwidth decreases as the distance increases and moreover the bandwidth is centered around the low frequencies. In Figure 3.6 it is also observed that the bandwidth is on the order of center frequency therefore an acoustic communication system can be accepted to be wideband as mentioned before.

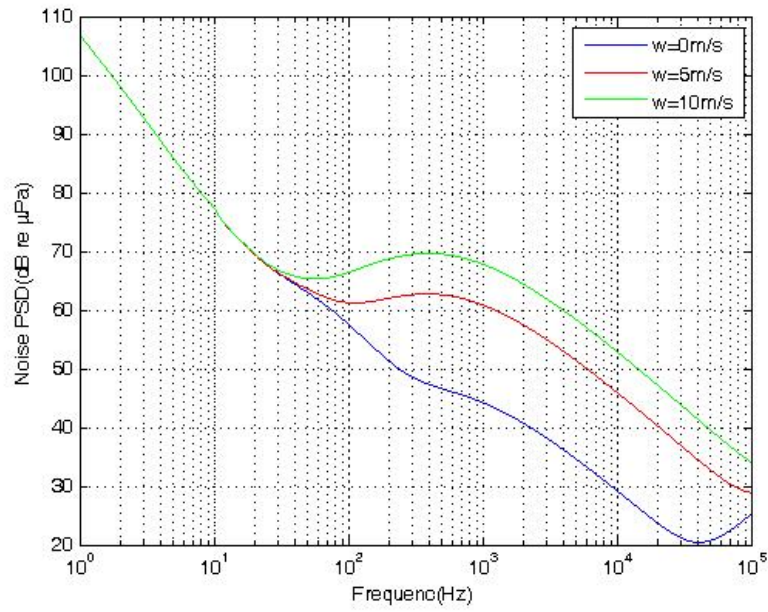


Figure 3.5: Noise Power Spectral Density for *ship activity*=0 and *wind speed*=0, 5, 10 m/s.

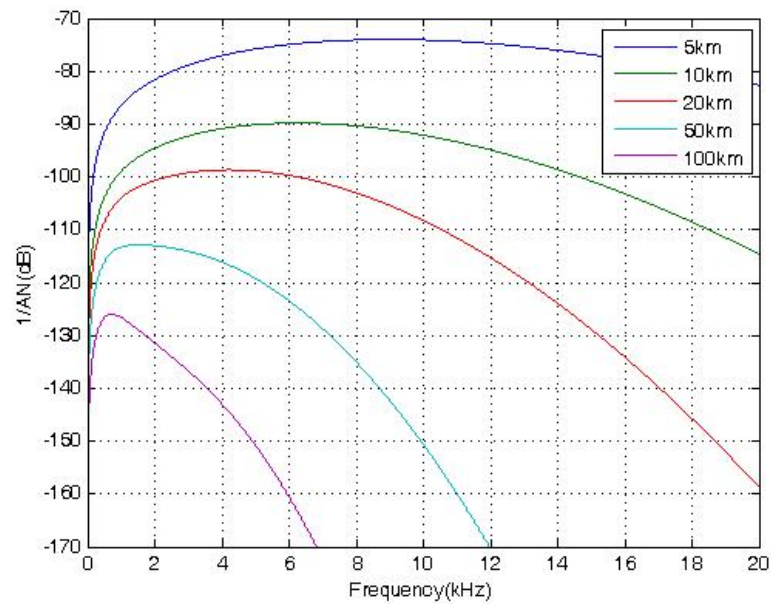


Figure 3.6: SNR depends on frequency and distance by the factor $1/A(r,f)N(f)$

3.4 Multipath [2, 3, 4]

Propagation of the acoustic signal occurs over multiple paths, therefore at the receiver side, multiple of transmitted signal with different amplitude, delay and phase are observed. This multipath phenomena causes distortion in the received signal since the received multipath signals interfere with each other. The multipath formation is result of reflection or refraction. The reflection and scattering of acoustic signal can be from the surface, bottom and any objects in the channel, in addition to that multipath can occur due to sound refraction in water. Sound refraction is a consequence of sound speed variation with depth, which is generally seen in deep water environment. The two formations of multipath in shallow and deep water are shown in Figure 3.1. The number of paths due to refraction changes due to environmental conditions such as pressure, temperature and density since the speed of sound depends on these factors [4]. In addition to that the number of multipaths depend on the geometry and physical properties of the channel therefore the channel impulse response differs from location to location even from time to time for the same location. The interference caused by multipath is time-varying and can be in such levels that the amplitude of the received signal can increase and decrease significantly in another word fades. The variability of the multipath is due to variability of the channel caused by temporal fluctuations such as internal and surface waves, turbulence, tidal flows and platform motion [2]. In a real underwater channel there can be infinitely many paths, however the ones that are below the noise level are ignored. Each path between the transmitter and receiver has its own spreading The total multipath spread is determined by the longest path or last arrived path.

The channel response can be obtained by adding all responses of multipaths which have different amplitudes, phases and delays. For a single path the channel response depends on the path length and frequency, since the arrival time and path loss depend on these variables.

3.4.1 Micro- and Macro-Multipath

The micro and macro multipaths are classified according to sources of their formation. The paths that are formed by slowly varying characteristic of the ocean are called macro-multipaths and the paths that are formed by rapidly varying characteristic of the ocean are called micro-multipaths. Therefore the channel is decomposed in two parts, the slowly varying, half-

deterministic part and rapidly varying, stochastic part [2].

Assuming that only first part of the ocean(half-deterministic part) is available and that the ocean surface is flat and the floor has only large scale features, the received signal's portion for a transmitted signal of $e^{j\omega t}$ in the l th path is given in (3.16). Here the large-scale or small scale terms are determined according to the spatial scales compared to acoustical wavelength. If a factor is bigger than the acoustical wavelength in spatial scale then it is large-scale or vice versa.

$$\tilde{R}_l(t, \omega) = H_l(t, \omega)e^{j\omega t}. \quad (3.16)$$

In (3.16) the function $H_l(\omega, t)$ is complex-valued and depends on slowly varying changes, speed of sound, large scale features of the sea floor and positions of the receiver and transmitter. Since $\tilde{R}_l(t, \omega)$ is the signal part which propagates along the l th path, $H_l(\omega, t)$ represents slowly varying phase delay and loss of the signal on that path only. The solid lines shown in Figure 3.1 construct *macro-multipaths structure* of the channel and are formed under the assumptions made above. The sound would not have to propagate along solid lines in Figure 3.1 if the assumptions made above are removed. In this situation the sound would be reflected and scattered from the small scale features of the ocean. Then the sound will propagate through a ray tube surrounding the rays defined by macro-multipath structure. These ray tubes are shown in Figure 3.1 as gray regions surrounding the solid lines.

If the fluctuations in the ocean have small amplitude or large spatial scale then the sound will propagate in the ray tube as a single disturbed path. This single path is divided into many micro paths in the ray tube as fluctuations' amplitude increases or their scale decreases. In this case the total portion of the received signal propagating in the l th ray tube is the sum of all micro paths in the l th ray tube. These micro paths constitute *micro-multipath structure* of the channel. Including the effects of rapid fluctuations and small scale environmental factors the portion of the received signal in the l th ray is obtained as follows:

$$R_l(t, \omega) = \Psi_l(t, \omega)\tilde{R}_l(t, \omega) = \Psi_l(t, \omega)H_l(t, \omega)e^{j\omega t} \quad (3.17)$$

where $\Psi_l(t, \omega)$ accounts for the effects of micro-multipath structure.

Assuming total of L rays between the transmitter and receiver the received signal, $R(t, \omega)$, for the transmitted signal of $e^{j\omega t}$ is obtained as follows:

$$R(t, \omega) = \sum_{l=1}^L R_l(t, \omega). \quad (3.18)$$

Rays between the transmitter and receiver generally do not overlap or have little overlap, thus unless the scale of the environmental fluctuations is on the order of rays' separation, the correlation between signal fluctuations due to micro-multipath in different rays is small.

The channel between the transmitter and receiver can also be characterized by using *input delay spread function*, $g(t, \tau)$. For this case the relationship between input and output is given as follows [2]:

$$r(t) = \int_{-\infty}^{\infty} g(t, \tau) s(t - \tau) d\tau, \quad (3.19)$$

where $s(t)$ is input and $r(t)$ is the output of the channel. In (3.19) it is seen that when input delay spread is not function of time then $g(t, \tau)$ reduces to time invariant impulse response. Let $R(\omega) = G(t, \omega)S(\omega)$ be the Fourier transform of the received signal where $G(t, \omega)$ and $S(\omega)$ are Fourier transforms of the input delay spread function and transmitted signal respectively. Then it can be easily shown that:

$$r(t) = \frac{1}{2\pi} \int_{-\infty}^{\infty} G(t, \omega) S(\omega) e^{j\omega t} d\omega. \quad (3.20)$$

Using linearity of the channel and (3.18) it can be shown that for the l th ray tube the received signal portion $r_l(t)$ is obtained as follows:

$$r_l(t) = \frac{1}{2\pi} \int_{-\infty}^{\infty} G_l(t, \omega) S(\omega) e^{j\omega t} d\omega. \quad (3.21)$$

Comparing (3.21) and (3.17) it is seen that $G_l(t, \omega) = \Psi_l(t, \omega)H_l(t, \omega)$. Therefore the input delay spread function of the l th ray tube using inverse Fourier transform is obtained as follows:

$$g_l(t, \tau) = \frac{1}{2\pi} \int_{-\infty}^{\infty} G_l(t, \omega) e^{j\omega \tau} d\omega = \frac{1}{2\pi} \int_{-\infty}^{\infty} \Psi_l(t, \omega) H_l(t, \omega) e^{j\omega \tau} d\omega. \quad (3.22)$$

Defining *micro-multipath input delay spread function*, $\psi_l(t, \lambda)$, of the l th ray tube and *macro-multipath input delay spread function*, $h_l(t, \lambda)$, of the l th ray as,

$$\Psi_l(t, \omega) = \int_{-\infty}^{\infty} \psi_l(t, \lambda) e^{-j\omega\lambda} d\lambda \quad (3.23)$$

$$H_l(t, \omega) = \int_{-\infty}^{\infty} h_l(t, \lambda) e^{-j\omega\lambda} d\lambda \quad (3.24)$$

(3.22) can be rewritten as convolution of $\psi_l(t, \lambda)$ and $h_l(t, \lambda)$ in the delay variable.

$$g_l(t, \tau) = \int_{-\infty}^{\infty} \psi_l(t, \lambda) h_l(t, \tau - \lambda) d\lambda \quad (3.25)$$

Finally, combining delay spread of all L rays, the channel input delay spread is obtained as follows:

$$g(t, \tau) = \sum_{l=1}^L g_l(t, \tau). \quad (3.26)$$

Input delay spread function of a channel with five paths is shown in Figure 3.7.

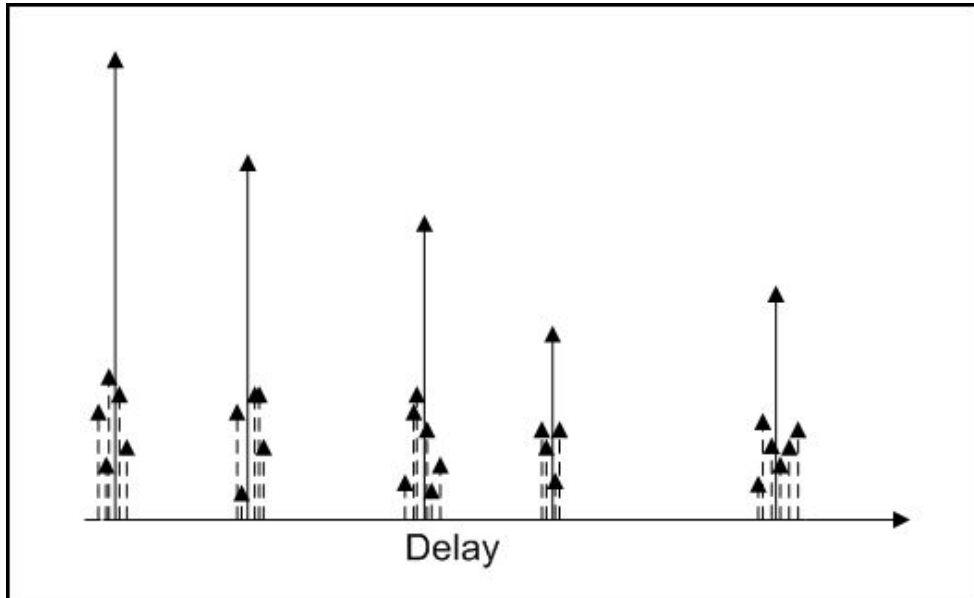


Figure 3.7: Input delay spread function for a channel with five paths

In Figure 3.7 the solid lines represent macro-multipath input delay spread function for each path and the surrounding shaded lines represent micro-multipath input delay spread function for each ray tube. Note that Figure 3.7 also represents response of the channel between the transmitter and receiver. In Figure 3.7 it is seen that macro-multipath structure determines the amplitude and delay of the cluster of arrivals and micro-multipath structure determines exact shape of the arrival for each ray tube. Note also that the micro-multipath structure of each ray tube is different therefore the shape of the arrivals and temporal spreadings are also different. Therefore the input delay spread function is clusters of taps in a tapped delay line. Each of these clusters accounts for a ray tube.

The saturation level of the channel provides information about spatial and temporal statistics of the channel. In case where the channel is unsaturated or partially saturated the tap weights within each cluster will be coherent. However when the channel is saturated the tap weights in a cluster will be independent due to incoherent fluctuation in the related ray tube. Moreover, if environmental fluctuations have spatial scales that are smaller than the separation between the ray tubes then the fluctuations of the tap weights in different clusters will be independent. This is due to fact that when the spatial scale of the environmental fluctuations is smaller than separation of ray tubes then there will be no overlap between ray tubes.

3.5 The Doppler Effect [3, 2]

Relative motion between transmitter and receiver and motion of the platform which transmitter and receiver stay on cause frequency shifting and frequency spreading which is known as Doppler Effect. The reason for that fact is that any change in the path length during propagation of the signal causes expansion (when the path increases) or compression (when the path decreases) of time axis in the received signal. Time axis change can be explained by the fact that due to path length change, delay of the signal changes and the leading and trailing part of the signal may have different delay values. This situation for the case where the path length increases is shown in Figure 3.8.

The level of Doppler effect is proportional to the ratio of relative speed between the transmitter and receiver to the speed of sound in the channel, that is $a = v/c$ where a is Doppler ratio, v is the relative speed and c is the speed of the sound. The speed of the sound in underwater

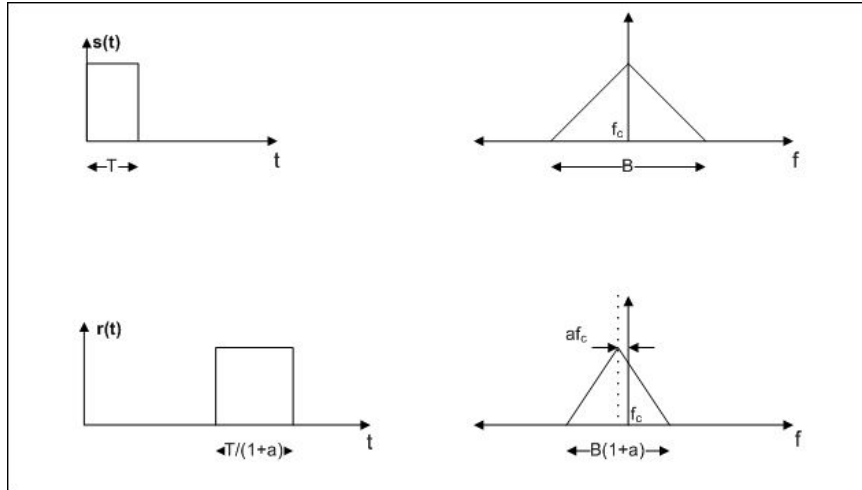


Figure 3.8: Doppler effect for the case where the path between the transmitter and receiver increases due to relative motion during the propagation of the signal. Upper part belongs to transmitted signal whereas the lower part belongs to received signal for a single path only. 'a' is Doppler ratio

channel is low (compared to speed of electromagnetic waves) and it is comparable to the relative speed between the transmitter and receiver. Moreover the speed of the platform, that is the speed of waves, currents and tides, is also comparable to the speed of sound. Therefore low propagation velocity of the sound in underwater channel can cause severe Doppler distortions [24].

Doppler effect created by relative motion between the transmitter or receiver can easily be calculated and removed from the received signal. However, Doppler effect created by platform motions cannot easily be calculated or estimated therefore it can be said that platform motions makes the Doppler analysis more difficult [11]. Furthermore as Doppler effect increases the coherence time of the channel decreases [10] since it was mentioned in Section 2.4.3 that the coherence time and Doppler spread are inversely proportional.

Considering only a single path for a single pulse $u(t)$ modulated with carrier frequency f_c the received signal is obtained as follows:

$$r(t) = s\left(t_0 + t - \frac{l(t_0) - vt}{c}\right) \quad (3.27)$$

where $l(t_0)$ is the path of the signal arrived at t_0 , v is the relative speed, t_0 is the reference time and $s(t) = \text{Re}\{u(t)e^{j2\pi f_c t}\}$. Letting $\tau = l(t_0)/c - t_0$ the received signal becomes as follows:

$$\begin{aligned}
r(t) &= s(t + at - \tau) = \text{Re}\{u(t + at - \tau)e^{j2\pi f_c(t+at-\tau)}\} \\
&= \text{Re}\{u(t + at - \tau)e^{j2\pi f_c(t+at)}e^{-j2\pi f_c\tau}\}.
\end{aligned} \tag{3.28}$$

In (3.28) it is seen that a phase of $e^{-j2\pi f_c\tau}$ has been added to the signal. Furthermore it is observed that the signal has been distorted in two ways. Firstly it has been scaled with $(1 + a)$ in time. This effect has been illustrated in Figure 3.8. In Figure 3.8 the signal duration has changed to $T/(1 + a)$ from T . Secondly a frequency offset of af_c has been added. The first distortion is referred to as *Doppler spreading* whereas the second one is referred as *Doppler shifting* [3]. Doppler shift is also referred to as the mean of frequency shift of the signal over some window of time [2]. If the mean is removed the remaining frequency fluctuations are Doppler spread. Doppler shift can be negative ($a < 0$) or positive ($a > 0$) according to the relative motion between the transmitter and receiver. If they get closer to each other positive Doppler shift ($a > 0$) is observed, however, if they get away from each other then negative Doppler shift is observed ($a < 0$). Since each ray tube has a different propagation path the Doppler shift can be different for different ray tubes.

In a straight-line propagation of the signal the relative speed generally describes the relative motion between the transmitter and receiver. However in underwater channel this is not valid since the sound propagates to the receiver after some reflections and refractions in the channel. The emission angle and arrival angle will be different from each other therefore the Doppler effect will be different due to motion of transmitter and receiver [16]. Let us consider the Doppler shift and the Doppler spread for the two situations for a single path. In the first one the transmitter moves towards the receiver and the receiver and the ocean is assumed to be fixed. Whereas in the second one the receiver moves away from the transmitter and the transmitter and the ocean are assumed to be fixed [16].

For the first case Doppler shift is

$$f_d = \frac{V_t f_c}{c_t} \cos(\alpha) = a_t f_c \cos(\alpha) \tag{3.29}$$

where α is emission angle, V_t is the velocity of the transmitter and c_t is the speed of the sound at the transmitter. The motion of the transmitter creates no frequency spread for a single ray tube [16]. For the second case the Doppler shift is obtained as follows [16]:

$$f_d = -\frac{V_r f_c}{c_r} \cos(\beta) = a_r f_c \cos(\beta) \quad (3.30)$$

where β is the angle of arrival, V_r is the speed of the receiver and c_r is the speed of the sound at the receiver side. At the receiver side each path or ray tube has different arrival angle therefore they cause different Doppler shifts. Micro-multipaths in each ray tube also have different angles of arrival. Assuming the arrival angle of micro-multipaths in the range $\pm 90^\circ$ around β the maximum and minimum Doppler shifts are obtained as follows [16]:

$$f_{dmax} = -\frac{V_r f_c}{c_r} \cos(90 + \beta) = -a_r f_c \cos(90 - \beta) = -a_r f_c \sin(\beta) \quad (3.31)$$

$$f_{dmin} = -\frac{V_r f_c}{c_r} \cos(0) = a_r f_c. \quad (3.32)$$

Therefore the frequency spread caused by Doppler shift in a single ray tube is obtained as $|f_{dmax} - f_{dmin}| = |a_r f_c (1 + \sin(\beta))|$. This frequency spread is centered around $f_c + a_r f_c \cos(\beta)$, that is around the frequency of the macro-multipath. Assuming a frequency spread of ocean B_o centered about the carrier frequency the total frequency spread is obtained as follows:

$$f_{spread} = B_o + |a_r f_c (1 + \sin(\beta))|. \quad (3.33)$$

When both of the transmitter and receiver are moving simultaneously the total Doppler shift is the sum of Doppler shifts caused by motions of the transmitter and receiver.

In a wideband system each frequency is shifted with different amount therefore the non-uniform frequency shift occurs.

3.6 Time Variability

There are two main sources of time variability of the underwater channel. First one is the natural sources and the second one is the motion of the transmitter or receiver. Natural sources can also be categorized as long term and short term factors. Among the latter ones the most important ones are the changes induced by the surface waves and the internal waves. Random signal

fluctuations(micro-multipaths) account for the time variability of the channel response. These random signal fluctuations are associated with each deterministic path (macro-multipath).

The reason for the fact that the most important contributor to time variability is the reflection of the sound from the waves is that motion of the reflection point results in a large frequency spread even much larger than that caused by other factors. In addition to that a dispersion of energy occurs when the reflection point moves. If there were no waves and the surface of the ocean was flat then the sound was going to reflect without any distortion but just a phase shift of π [22]. Vertical motion of the ocean surface can be modeled as a zero mean Gaussian random variable, where the power spectrum of the random variable will depend only on the speed of the wind [22]. For a signal with frequency f , arrival angle of θ for a single reflection from the surface the Doppler spread is $(0.0175/c)fw^{1.5}\cos(\theta)$ where c is the speed of the sound and w is speed of wind [22]. Doppler spread decreases as the distance between the transmitter and receiver increases, since lower frequencies will be used for long distance transmissions, on the other hand multipath delay spread will increase. However the channel spread factor which is the product of Doppler and multipath spread is expected to decrease [22]. A time-varying multipath channel generally is modeled as a tapped delay line. The gains of the taps are modeled as stochastic processes with certain power spectral densities and distributions. Moreover the spaces between the taps are taken as the inverse of twice the channel bandwidth [22]. The underwater acoustic channel are commonly modeled as Rayleigh fading channel [16, 9, 25]. However there is no single model accepted for underwater acoustic channel. Even some authors have modeled underwater acoustic channel as a deterministic model [26].

CHAPTER 4

SIMULATION OF UNDERWATER CHANNEL

4.1 Introduction

The test and research operations in underwater channel is expensive, time taking and quite difficult. Therefore a reliable and accurate model of the underwater channel will be very helpful for underwater research, test and other purposes. The model should encounter all physical properties of the underwater channel mentioned in Chapter 3, since identifying the medium quantities and physical properties of the channel is the most important step in simulation of the underwater channel. The model will be more reliable and acceptable as it uses more physical parameters simultaneously.

In this simulation model following parameters will be used as input parameters:

- Depth of the water
- Depth of the transmitter and receiver
- Horizontal distance between the transmitter and receiver,
- Carrier frequency
- Speed of the transmitter and receiver
- Sea state and wind speed
- Roughness of the bottom
- Temperature

- Salinity

Depth of the water will be used to determine number of paths and the length and destination of the paths. In addition to that deep water and shallow water characteristics are different from each other. In order to calculate the number of paths and the route of the paths, depth of the transmitter and receiver, sea state and wind speed, horizontal distance and roughness of the bottom parameters are also necessary. Delay of each path will be calculated using route of the path and the speed of the sound in that path, for this reason temperature, depth and salinity are necessary parameters. Doppler effect will be calculated by using speed of the transmitter and receiver and sea state variables. The loss during propagation of the signal on each path will be calculated by using the route of the path and the carrier frequency. In addition to that depth of the water will determine spreading loss type, to which range spherical and cylindrical spreading will be used. Moreover to find exact loss during propagation of the signal, reflection loss and reflection coefficient should also be used for each reflection. The background noise should be added to the propagating signal. The background noise depends on the frequency and site of the channel. Therefore using input parameters given above the following properties of the channel will be calculated:

- Number of multipaths(direct,bottom,surface)
- Delay for each path
- Doppler effect for each path(including Doppler shift, frequency spread and signal duration change)
- Loss for each path(includes spreading and absorption loss)
- Reflection loss and coefficient for each path(include surface and bottom reflection coefficient and loss with grazing angles)
- Distance traveled for each path
- Background noise
- Speed of sound for the given environment

4.2 Ambient Noise Generation

Time domain noise signal has been generated by using white Gaussian noise and FFT and IFFT transforms. The main idea in creating a noise signal with known PSD is that when a signal $x(t)$ is filtered by $h(t)$ the the output signal $y(t)$ will have a power spectral density $S_y(f) = S_x(f)|H(f)|^2$ where $H(f)$ is the frequency response of the filter, $h(t)$. This is illustrated in Figure 4.1.

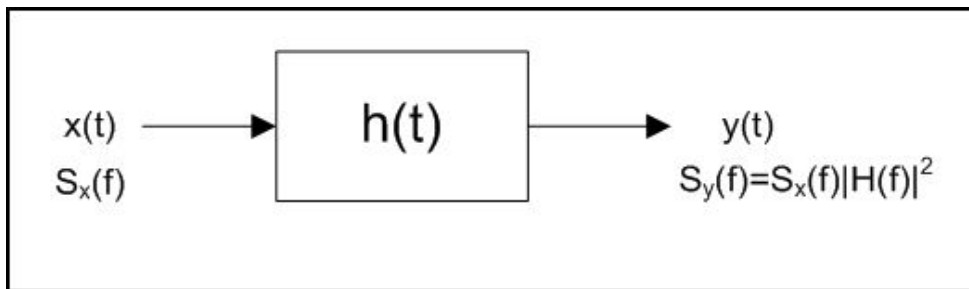


Figure 4.1: PSD relation between input and output of a filter

In addition to that it is known that the PSD of the white Gaussian is flat, therefore to have a noise with known PSD, the white Gaussian noise can be filtered through a filter whose frequency response square equals to the known PSD. Then the output signal will have a desired PSD. Moreover, convolution in time domain equals to multiplication in frequency domain. Considering these facts underwater ambient noise is generated as shown in Figure 4.2.

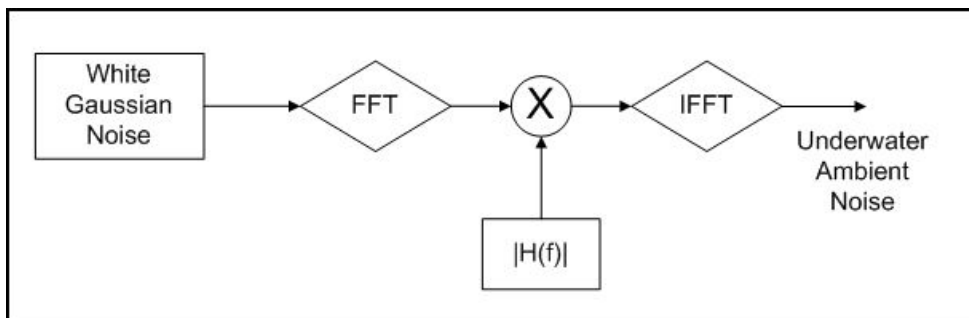


Figure 4.2: Underwater ambient noise generation by using white Gaussian noise

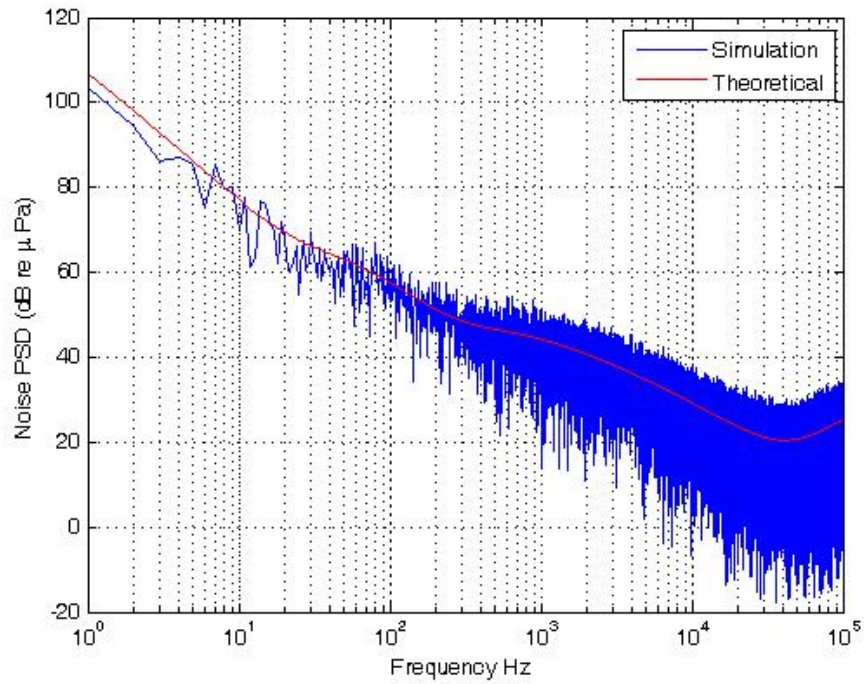


Figure 4.3: Theoretical and simulated underwater ambient noise Power Spectral Densities for wind speed=0 m/s

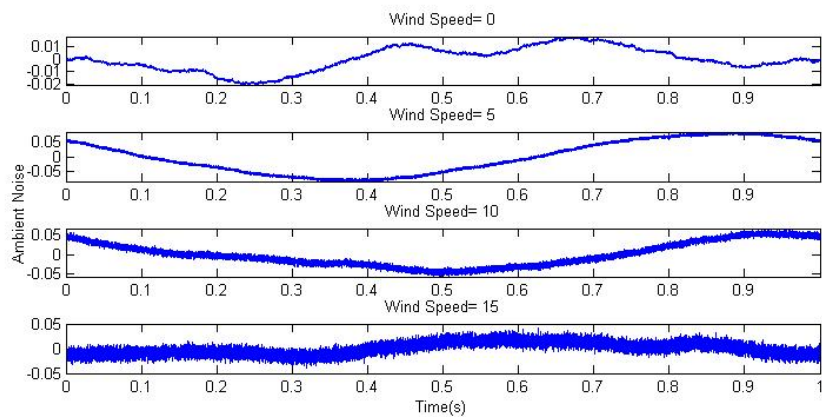


Figure 4.4: Time domain ambient noise signal

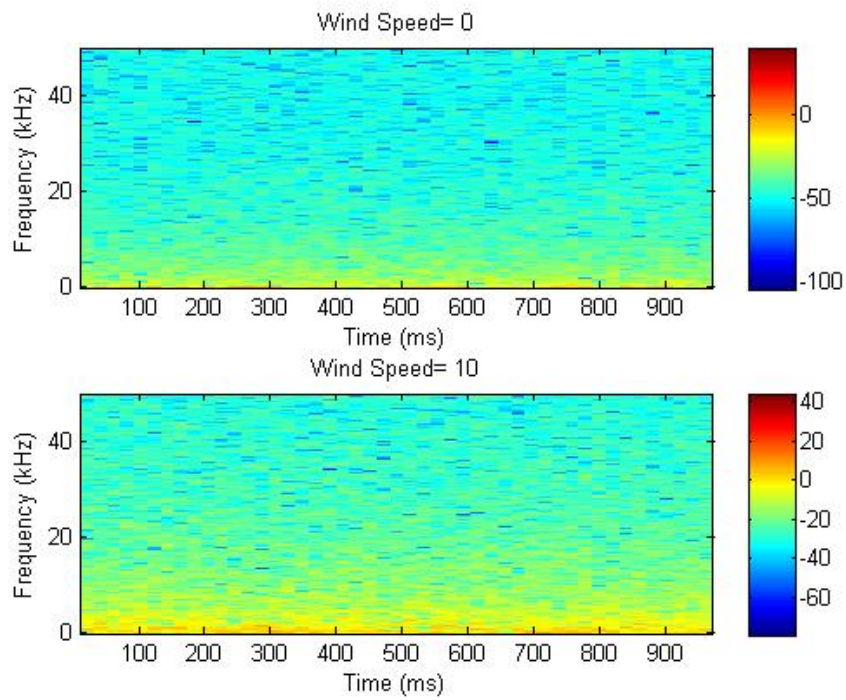


Figure 4.5: Spectrogram of ambient noise for wind speeds 0 and 10 m/s

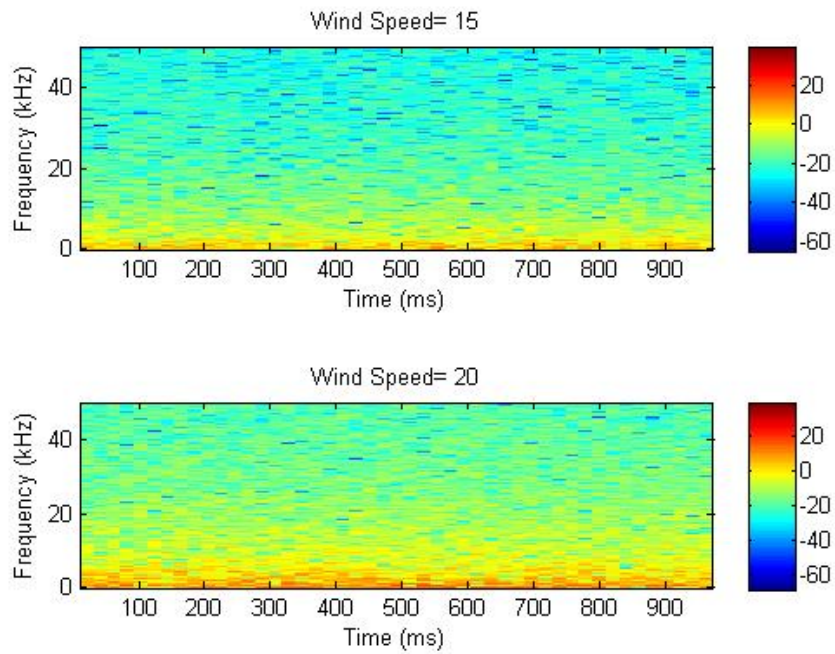


Figure 4.6: Spectrogram of ambient noise for wind speeds 15 and 20 m/s

The PSDs of the generated ambient noise and theoretical ambient noise are shown in Figure 4.3. The time domain signal of the ambient noise for wave speed equals to $0m/s$, $5m/s$, $10m/s$ and $15m/s$ is seen in Figure 4.4. The spectrogram of the ambient noise for different wind speeds is plotted in Figure 4.5 and 4.6. Here, it should be noted that while obtaining the ambient noise, it is assumed as a WSS and linear process.

4.3 Time Delay and Received Power

The multipaths from transmitter to the receiver have different time delays. The delay can severely increase due to paths that reach to the receiver after scattering from the surface and bottom a few times. The paths having different delay times are shown in Figure 4.7, note that the loss is ignored in Figure 4.7 in order to observe the delays clearly.

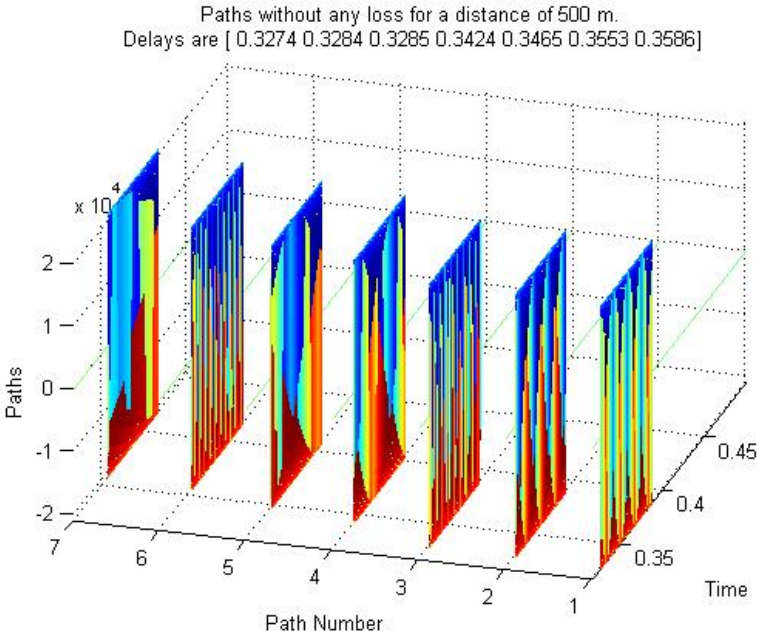


Figure 4.7: Received signals from different paths with different delay times; losses are ignored.

The physical conditions for which the Figure 4.7 is obtained are given in Table 4.1

Note that all of the paths are not given, only the first 7 paths arriving the receiver are shown in Figure 4.7. The signal is sent from the transmitter at $t = 0$.

Table 4.1: The physical conditions for Figure 4.7

Depth (m)	Horizontal Distance (m)	Signal Frequency (kHz)	Transmitter Depth (m)	Receiver Depth (m)	Signal Duration (ms)
100	500	10	10	35	20

The received signal and its received power for the condition given in Table 4.1 and for the case where all conditions are the same but the horizontal distance changed to 200m are seen in Figure 4.8 and Figure 4.9, respectively.

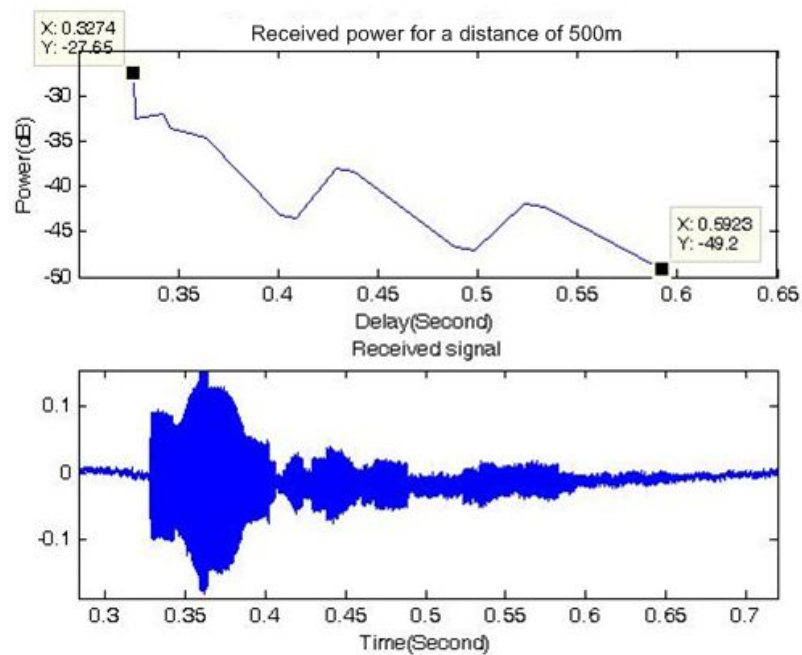


Figure 4.8: Received power and the received signal for 500 m horizontal distance

In Figure 4.8 and 4.9 the delay spread can be calculated as about 0.27s for 500m and 0.38s for 200m cases. Remember that the delay spread is the time difference between the first and the last arrival. Therefore the relative time is the variable of interest. The relative times with respect to the first arriving path for two different horizontal distances 500m and 200m are plotted in Figure 4.10.

As it is seen in Figure 4.10 that the relative time for smaller distances are bigger. This is an

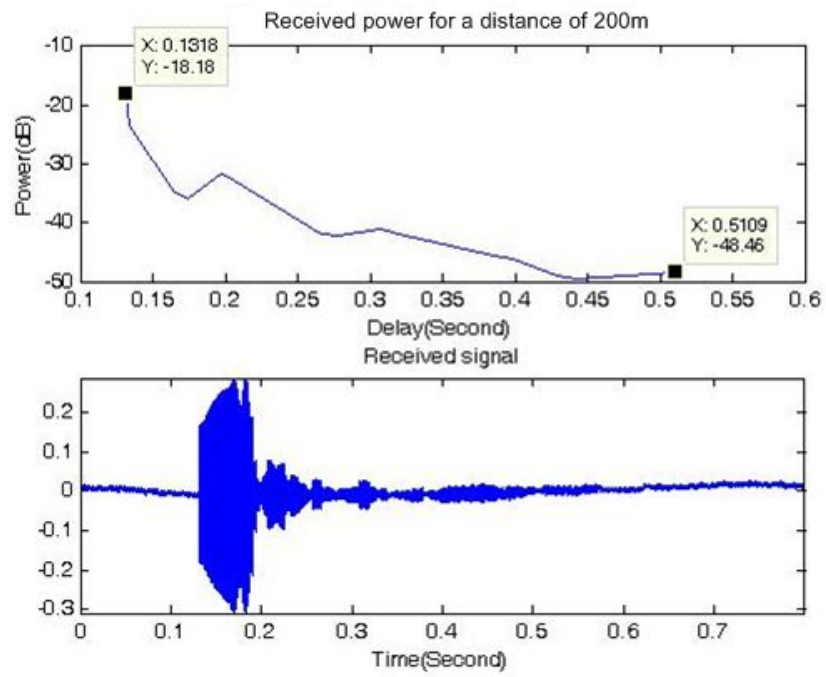


Figure 4.9: Received power and the received signal for 200 m horizontal distance

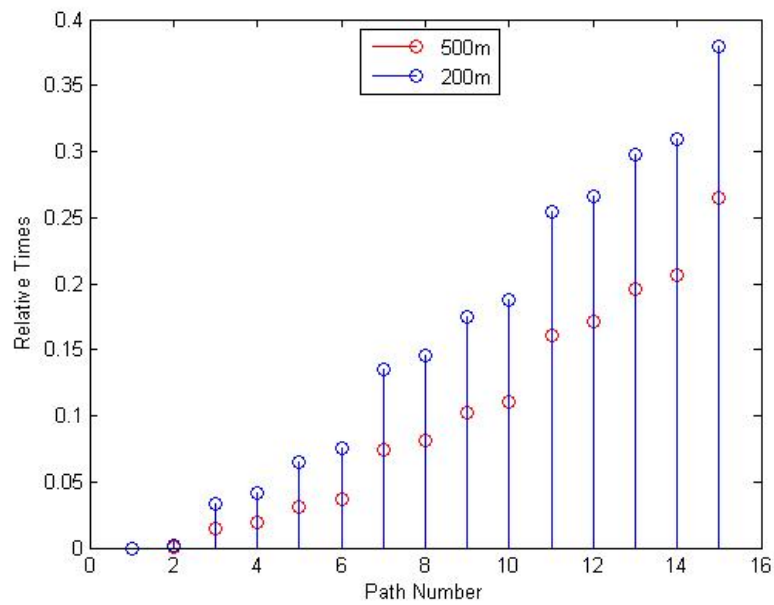


Figure 4.10: Relative times for 200m and 500m distances

expected result since as the horizontal distance between the transmitter and receiver increases the traveled distances for different paths get close to each other. Therefore, the delay spread decreases as the distance between the transmitter and the receiver increases. In particular, if the signal for this situation is assumed to be a symbol, ISI will be bigger for longer distances.

4.4 Doppler Spread and Doppler Power Spectrum

When there is a relative motion between the transmitter and the receiver Doppler effect is observed. The spectrogram of the received signal for the case where the transmitter speed is $2m/s$ and the receiver speed is $3m/s$, is shown in Figure 4.11. The receiver and the transmitter are getting closer to each other, so the relative motion is $+5m/s$. Therefore the Doppler shift for all paths will be positive. This fact is observed in Figure 4.11. The input frequency in Figure 4.11 is $10KHz$.

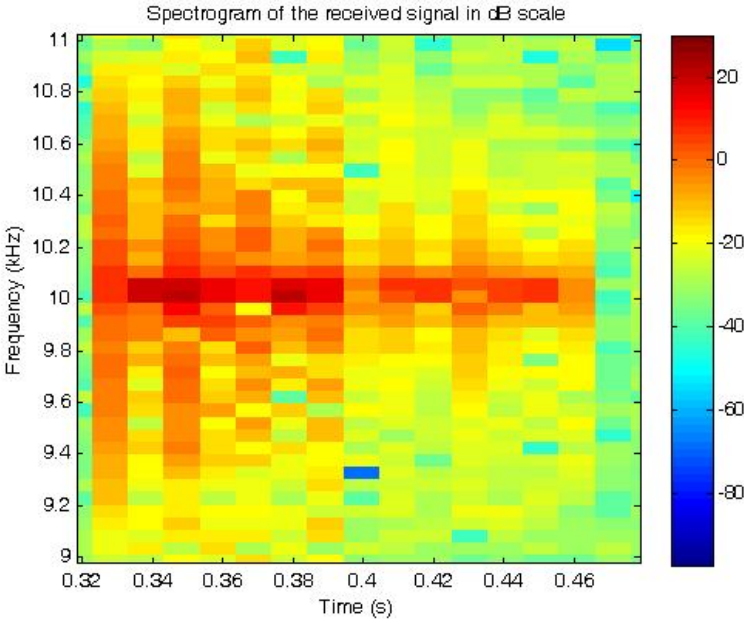


Figure 4.11: Doppler shifts in the received signal, where the input frequency is 10KHz

For the same conditions mentioned above the Doppler power spectrum is obtained as in Figure 4.12.

As described in Section 2.4.3, the Doppler spread can be found by using Doppler power

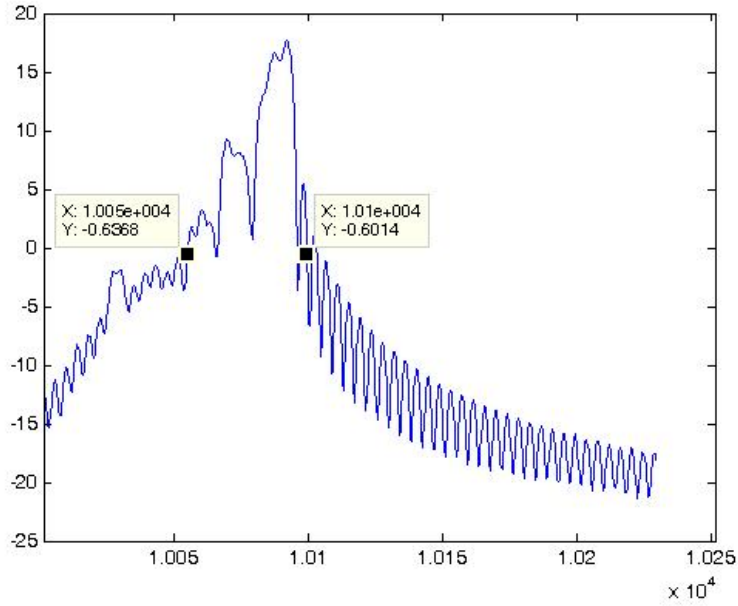


Figure 4.12: Doppler power spectrum for a relative motion of +5m/s

spectrum. The Doppler spread is found to be about 50Hz from Figure 4.12.

4.5 Loss

In Section 3.3, spreading loss, absorption loss and scattering loss, and their mechanisms were described. Spreading loss depends on the traveled distance and absorption loss greatly depends on the frequency of the sound. On the other hand, scattering loss greatly depends on the physical properties of the channel, grazing angle of the sound, and the type of the bottom. There are different models for scattering loss [27]. Here, for the surface scattering loss *Beckmann-Spizzichino Surface Loss* model and for bottom scattering loss *HFEVA (High Frequency Environment Acoustic)* model are implemented. In *Beckmann-Spizzichino Surface Loss* model, the surface loss SL is given in (4.1).

$$SL = 20\log(C_v - C_s) \quad (4.1)$$

where C_v and C_s are given as:

$$C_v = \sqrt{1 - \sin(\phi) + \frac{\sin(\phi)\exp(-T)}{\phi \sqrt{\pi\sigma}}}$$

$$C_s = 0.3 + \frac{0.7}{1 + 0.01(1.1610^5 f w^2)} \quad (4.2)$$

under the constraint that

$$\frac{\sin(\phi)}{2} \leq \left[\sin(\phi) - \frac{\sin(\phi)\exp(-T)}{\phi \sqrt{\pi\sigma}} \right] \leq 0.99 \quad (4.3)$$

where f , ϕ and w in (4.2) are frequency in *Hz*, grazing angle in *rad* and wind speed in *kts* respectively and σ and T are given as follows:

$$\sigma = \frac{500}{3 + 2.6w}$$

$$T = \frac{\sigma\phi^2}{4} \quad (4.4)$$

The bottom loss in HFEVA model is computed as follows:

$$BL = -20 \log_{10} \text{abs}(R(\theta))$$

$$R(\theta) = y - 1y + 1$$

$$y = \frac{\rho \sin(\theta)}{P(\theta)} \quad (4.5)$$

$$P(\theta) = \sqrt{[\kappa^2 - \cos(\theta)]}$$

$$\kappa = \frac{1}{\nu(1 + i\delta)}$$

where θ is the grazing angle and δ , ν and ρ are loss parameter, sound speed ratio and density ratio of the bottom, respectively, and are given for different types of bottom in [27]. It is seen that the surface and bottom loss greatly depend on the grazing angle.

The first seven paths' signals subject to only spreading and absorption losses are shown in Figure 4.13

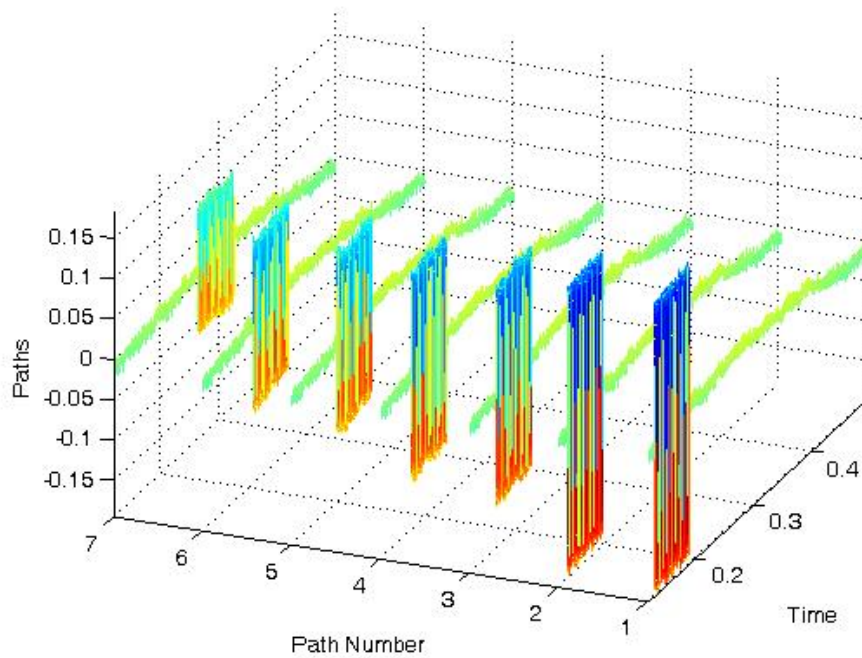


Figure 4.13: Paths with spreading and absorption loss mechanisms only

The first seven paths subject to all loss including bottom and surface loss are in Figure 4.14. Note that the bottom type is taken as coarse sand in getting these results.

When Figures 4.13 and 4.14 are examined it is seen that surface and bottom losses are larger than spreading and propagation losses. Therefore the sound can propagate to longer distances when there is no surface and bottom scattering, that is when the sound is trapped in a sound channel.

4.6 Multipath Formation and Micropath Effect

The multipaths used in simulation are formed in two ways. In a realistic underwater environment the multipaths can reflect from any point in between the transmitter and the receiver. Some multipaths are reflected only once whereas some multipaths can have multiple of reflections. Therefore to simulate a more realistic multipath formation two ways are used for multipath formation. In the first way the multipaths' reflection points are randomly chosen between the transmitter and the receiver from both surface and bottom. The paths formation

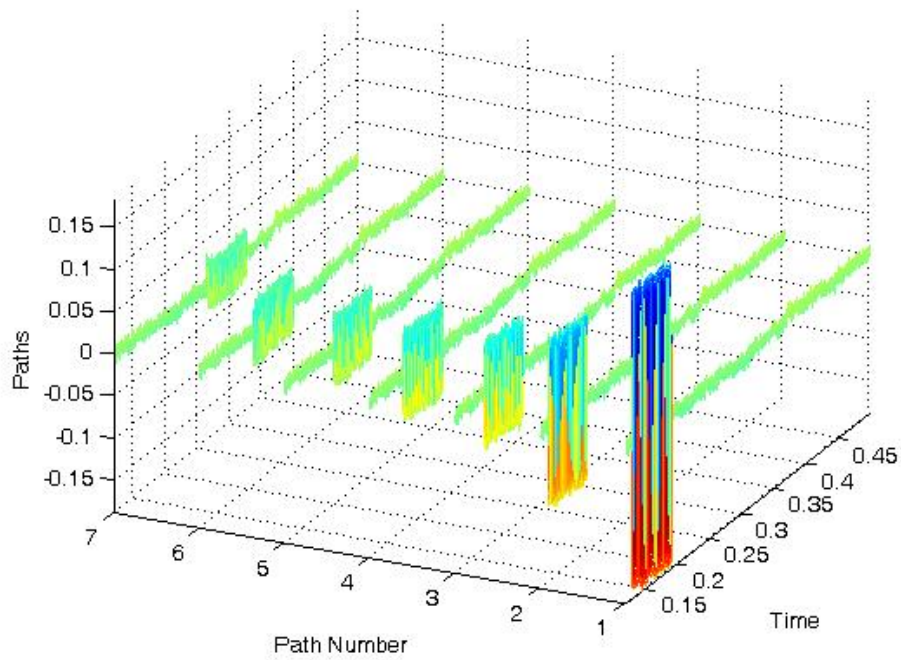


Figure 4.14: Paths with all loss mechanisms

for the first way is shown in Figure 4.15.

In the second way the images of multipaths are formed by assuming the surface and bottom like a reflector or mirror. The second way is used for having multiple reflections. In the second way therefore the surface and bottom are accepted as flat. The path formation for the second way is shown in Figure 4.16. In the second method only first two paths have one reflection, the remaining ones reach receiver after at least two reflections. Note that Figure 4.16 shows only the first four paths in the second method. In the first method the losses are smaller therefore the amplitude of the received signal is mostly determined by the first method, whereas in the second method delays are larger therefore the second method contributes more to signal extension and delay spread.

In Section 3.4.1 it was mentioned that the channel can be divided to rapidly changing and slowly changing parts. The micropaths are the result of rapidly changing part of the channel or small-scale terms in the channel. In Figures 4.7, 4.13 and 4.14 the micropath effect is neglected, that is the paths propagate in a straight line but not in a ray tube. If the effect of the

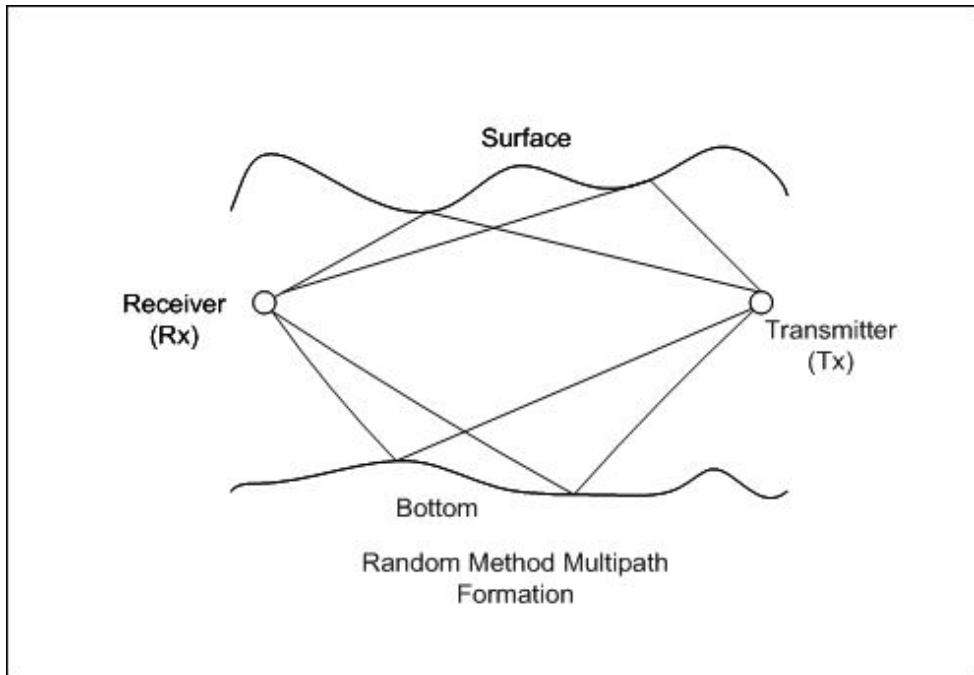


Figure 4.15: Random method multipath formation

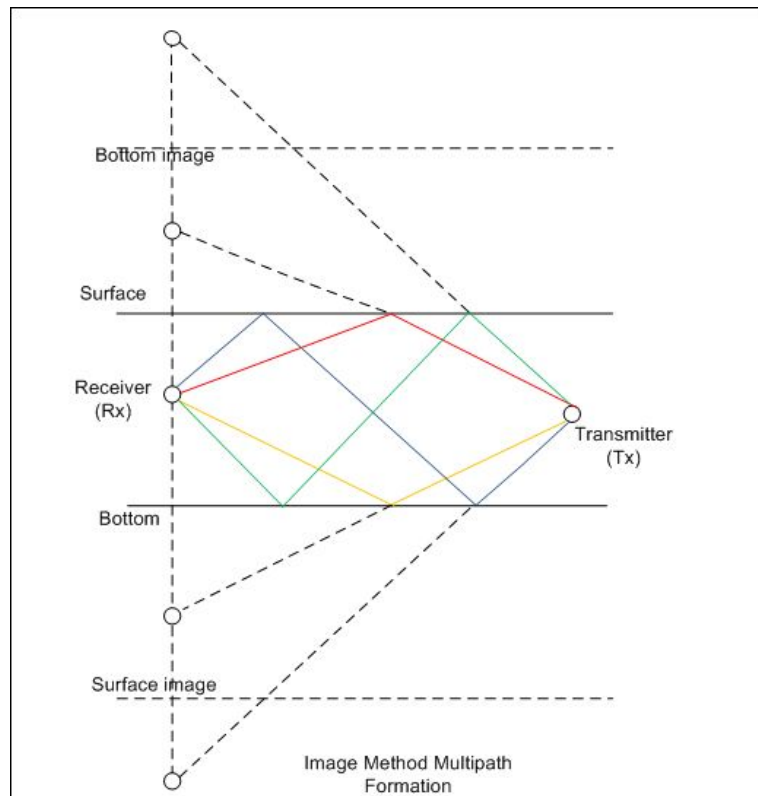


Figure 4.16: Image method multipath formation

rapidly varying and small-scale characteristics of the channel are included then the paths are obtained as shown in Figure 4.17.

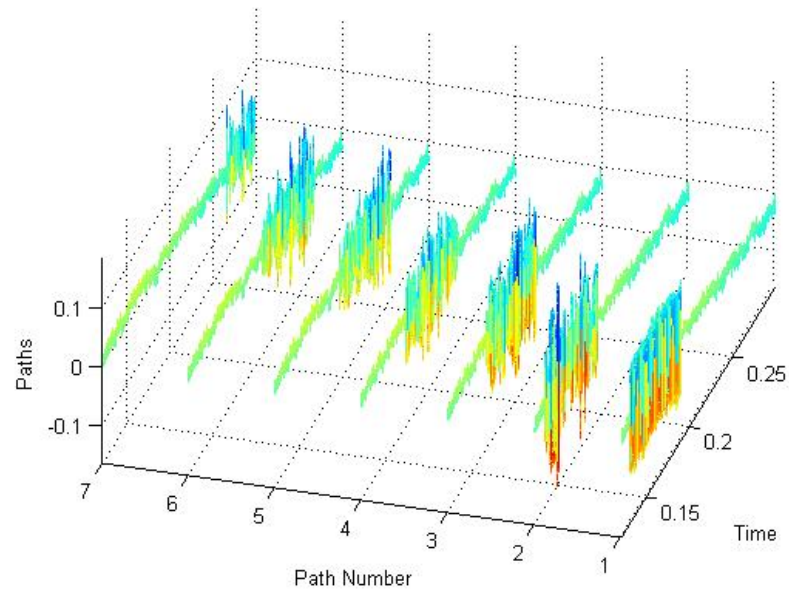


Figure 4.17: Micropath effect is seen on the paths. Note that there is no micropath effect on the first path

In Figure 4.17 in the paths that are subject to micropath, even though the delay and significant path loss have not changed, very fast fluctuations are observed in the paths' amplitudes. The micropath effect is simulated as shown in Figure 4.18 [16].

In Figure 4.18 the low-pass filters are matched and their bandwidth is total frequency spread (Doppler effect and frequency spread due to sea motion) of each multipath. The Gaussian noises used are zero mean and unit variance [16].

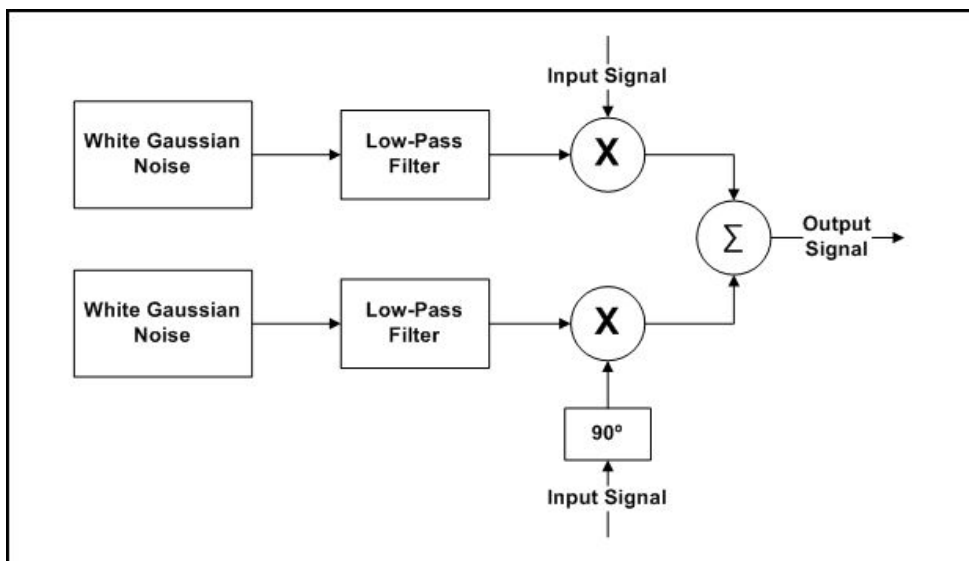


Figure 4.18: Micropath effect simulator

CHAPTER 5

MODEL FITTING TO EXPERIMENTAL DATA

This chapter is removed.

5.1 Introduction

5.2 Optimization of Channel Parameters

5.2.1 Optimizing the Sound Speed

5.2.2 Optimizing the Number of Paths

CHAPTER 6

CONCLUSION

In this thesis an underwater channel simulation and parameter optimization is conducted. Firstly a general literature review has been done about multipath fading channels, underwater physical properties and existing underwater channel models. The mathematical models of these concepts are determined and used for simulation purpose. Secondly a channel model is implemented in which nearly all physical properties of underwater environment including randomness, Doppler effect and inherent inhomogeneities of the underwater environment are modeled. Finally the model parameters are optimized by the help of experimental data for specific scenarios.

The missing knowledge of the transmitter side and phase forced us to conduct the channel identification in frequency domain, however, to obtain a good result the identification procedure should be conducted in time domain. The magnitude operation also decreases the performance of channel identification, since instead of matching complex and real parts the magnitude is matched, and the magnitude can be the same for different signals having different complex and real parts. In addition to that, nonlinear part of underwater channel are neglected. The channel is assumed as a WSS and linear channel.

6.1 Results

Underwater channel is a dynamic and continuously changing environment. There is no such a channel impulse response that can be used for every underwater channel but rather there are lots of versions of underwater channel impulse response specific to each local zone and day time. This is because a little fluctuation in temperature, wind speed, noise and other factors

that effect underwater environment results in a completely different channel impulse response.

The attenuation in underwater environment does not depend only on distance but also on frequency, temperature, salinity and depth as well. The frequency increase results in attenuation increase whereas the temperature and salinity increase results in attenuation decrease. On the other hand, depth increase results in attenuation decrease. Moreover since there is no reflection loss in deep water the propagation distance of deep water is greater than that of shallow water. The attenuation increase due to frequency increase obligates to use low frequencies in underwater systems. Moreover since it is necessary to work at low frequencies and bandwidth is comparable to carrier frequency underwater channels are accepted to be wideband.

Surface and bottom reflections with refractions due to inhomogeneity of sound speed cause propagation of the transmitted signal to the receiver over multipaths. The number of multipaths are completely random and are actually very large but the ones under noise level are ignored and the ones that have very close delay can be accepted as one multipath. If there was not multipath effect in underwater systems the stochastic property of the channel was going to decrease and moreover the complexity of the channel was going to decrease. In this situation the only path that the transmitted signal propagates was going to be direct path and that path was going to be characterized by just a nearly determined loss and delay. Therefore, the complexity and difficulty of the channel is mostly due to multipath effect.

The simulated channel characterization functions seem to be not consistent very well with that of real channel for the same physical conditions. In addition that the decision of number of paths parameter was difficult. Therefore an optimization of number of paths was necessary. Moreover, it was found that for the given real channel the temperature and salinity are not known therefore the sound speed that will be determined theoretically would not agree exactly to the real one since the temperature and salinity parameters used for theoretical calculation was going to be average values. Hence an optimization procedure is implemented for both of these variables. It was found that after optimization procedure the characterization functions were more consistent for simulated and real channel. For number of paths optimization it cannot be said that the obtained number is exactly giving the number of paths that the transmitted signal propagates, however it can be said that the simulated channel best fits to real channel under these number of paths.

Table 6.1: The scenarios for the planned measurement

Scenario	Horizontal Distance	Frequency (kHz)	Signal	Transmitter Depth (m)	Receiver Depth (m)
1-Depth 15m	Short, Medium, Long	At least 3 different bands	FM, CW, Noise, Pulse	5, 10, 15	5, 10, 15
2-Depth 50m	Short, Medium, Long	At least 3 different bands	FM, CW, Noise, Pulse	25, 35, 50	25, 35, 50
3-Depth 100m	Short, Medium, Long, Very Long	At least 3 different bands	FM, CW, Noise, Pulse	60, 75, 100	60, 75, 100
4-Depth 250m	Short, Medium, Long, Very Long	At least 3 different bands	FM, CW, Noise, Pulse	150, 200, 250	150, 200, 250

6.2 Future Work

As future work residual signal in the channel can be modeled which is not included in the existing model. Moreover effects of the transducers can be studied and added into model. In the designed model only horizontal motion of receiver and the transmitter is modeled, vertical motion of the transmitter and receiver can also be modeled.

In order to test the proposed model in a better way and to investigate underwater channel in more detail some measurements are planned. The scenarios for the measurement are given in Table 6.1.

The measurements are planned to be conducted in different locations and in different seasons.

REFERENCES

- [1] A. Goldsmith. *Wireless Communications*. Cambridge University Press, Cambridge, 2005.
- [2] H. V. Poor and G. W. Wornell. *Wireless Communication Signal Processing Perspectives*, chapter 8: Underwater Acoustic Communications. Prentice Hall, New Jersey, 1998.
- [3] M. Stanjovic. Underwater Acoustic Communications: Design Considerations on the Physical Layer. *Wireless on Demand Network Systems and Services. WONS 2008. Fifth Annual Conference*, 2008.
- [4] J. Preisig and M. Stanjovic. Underwater Acoustic Communication Channels: Propagation Models and Statistical Characterization. *IEEE Communication Magazine*, January 2009.
- [5] Z. Jiang. Underwater Acoustic Networks: Issues and Solutions . *International Journal of Intelligent Control and Systems*, 13:152–161, Sep 2008.
- [6] M. Stanjovic. Recent Advances in High-speed Underwater Acoustic Communications . *IEEE Journal Of Oceanic Engineering*, 21:125–136, april 1996.
- [7] A. B. Baggeroer, J. C. Preisig, and T. H. Eggen. Communication Over Doppler Spread Channels Part I: Channel and Receiver Presentation. *IEEE Journal Of Oceanic Engineering*, 25:62–71, January 2000.
- [8] M. Chitre. A High-Frequency Warm Shallow Water Acoustic Communications Channel Model and Measurements. *Acoustical Society of America*, November 2007.
- [9] R. Galvin and R.F.W. Coates. A Stochastic Underwater Acoustic Channel Model. *IEEE OCEANS*, 1:203–210, Sep 1996.
- [10] W. B. Yang and T. C. Yang. Characterization and Modeling of Underwater Acoustic Communications Channels for Frequency-Shift-Keying Signals. *IEEE OCEANS*, pages 1–6, September 2006.
- [11] G. Bertolotto, P. V. Walree, and T. Jenserud. Initial Design of an Acoustic Communication Channel Simulator. *RTP 110.060 UUV Covert Acoustic Communications Project*, 2007.
- [12] H. P. Bucker and M. B. Porter. Gaussian Beam Tracing for Computing Ocean Acoustic Fields. *J. Acoust. Soc. Am.*, 82:1349–1359, 1987.
- [13] A. Sehgal. Analysis and Simulation of the Deep Sea Acoustic Channel for Sensor Networks. Master’s thesis, Jacobs University, Bremen, Germany, 2009.
- [14] A. Bouzoualegh, Th. Val, E. Campo, and F. Peyrard. Modelling and Simulation of Underwater Acoustic Communication Based on Stateflow and Simulink Models. *SETIT*, March 2005.

- [15] M. A. M. Gutierrez, P. L. P. Sanchez, and J. V. V. Neto. An Eigenpath Underwater Acoustic Communication Channel Simulation. *OCEANS, 2005. Proceedings of MTS/IEEE*, 1:355–362, 2005.
- [16] A. Zielinski and X. Geng. An Eigenpath Underwater Acoustic Communication Channel Model. *OCEANS '95. MTS/IEEE. Challenges of Our Changing Global Environment. Conference Proceedings.*, 2:1189 – 1196, January 1995.
- [17] R. Pattarkine. High Rate OFDM Acoustic Link for Underwater Communication. *PVGs College of engineering and Technology*, November.
- [18] B. Sklar. Rayleigh Fading Channels in Mobile Digital Communication Systems. *IEEE Commun. Mag*, 35(7):90–100, July 1997.
- [19] L. M. Brekhovskikh and Y. P. Lysonov. *Fundamentals of Ocean Acoustics*. Springer-Verlag, Berlin, 1991.
- [20] Y. L. Sun and Z. Han. Cooperative Transmission for Underwater Acoustic Communications. *IEEE International Conferences on Communication*, May 2008.
- [21] E. M. Sozer, J.G. Proakis, and M. Stojanovic. Underwater Acoustic Networks. *IEEE Journal of Oceanic Engineering*, 25(1), January 2000.
- [22] M. Stojanovic. Underwater Acoustic Communication. Quart. Progr. Rept., Entry For the Wiley Encyclopedia of Electrical and Electronics Engineering, 1999.
- [23] P. King, R. Venkatesan, and C. Li. Modeling a Shallow Water Acoustic communication Channel Using Environmental Data for Seafloor Sensor Networks. *Wireless Communications and Mobile Computing*, OCT 2009.
- [24] A. C. Singer, J. K. Nelson, and S. S. Kozat. Signal Processing For Underwater Acoustic Communications. *IEEE Communication Magazine*, 47:90 – 96, January 2009.
- [25] Z. Guoqing and S. Taebo. Simulation Analysis of High Speed Underwater Acoustic Communication Based on a Statistical Channel Model. *Image and Signal Processing, 2008. CISP '08.*, 5:512–517, May 2008.
- [26] A. Essebbar, G. Loubet, and F. Vial. Underwater Acoustic Channel Simulations for Communication. in *OCEANS '94 Proc*, 3:495–500, Sep 1994.
- [27] R.P. Hodges. *Underwater Acoustics: Analysis, Design and Performance of Sonar*. Wiley, West Sussex, 2010.